Graz University of Technology

Bachelor's Thesis

Prevention of Flutter Echoes in Architecturally Demanding Spaces

Electro Acoustics and Room Acoustics Seminar

conducted at the
Signal Processing and Speech Communications Laboratory
Graz University of Technology, Austria

by
Peter Maximilian Giller

Supervisor:
Dipl.-Ing. Jamilla Balint

Graz, July 2, 2015

Abstract

This bachelor thesis deals with the problem of flutter echoes inside enclosed spaces and possible measures to prevent them. Flutter echoes result from repeated sound reflections between parallel walls with insufficient absorption; they are mostly perceived as disturbing and can noticeably impair speech intelligibility.

After a summary of some theoretical fundamentals of acoustics and measurement techniques, measurements are performed in the interior space of the university building Inffeldgasse 16 c, Graz, regarding the general acoustic situation and the flutter echoes in the building. Trying to find valid measures for the whole space and to detect the echoes in the measured impulse responses, different problems resulting from the size and the shape of the building were encountered.

A simulation of the whole building in *CATT-Acoustic* was created. The comparison with the measurement data shows significant differences, which again can likely be traced back to the room geometry.

Finally, various possible strategies for prevention of flutter echoes, both in general and with regard to the situation in the examined enclosure, are presented and reviewed by means of simulations.

Statutory Declaration

I declare that I have authored this thesis independently, that I have not used other than the declared sources/resources, and that I have explicitly marked all material which has been quoted either literally or by content from the used sources.

date	(signature)

Contents

List of Figures

1 Introduction

Room acoustical measures are often neglected in the architectural design process of new buildings. Especially in office spaces, this can lead to significant disturbances in everyday work. Modern concepts are often based on clear shapes and orthogonal elements. In a minimalist design, the extensive use of sound-hard materials like concrete and glass often leads to unpleasant phenomena like poor speech intelligibility due to long reverberation times, or flutter echoes.

This thesis deals with the problem of flutter echoes and possible measures to prevent them. Improvement measures will be designed to avoid flutter echoes, even if the possibilities for using acoustically effective materials are very limited due to visual reasons.

The problems described above can be found at the university building Inffeldgasse 16 c. This building will serve as an example for measurements with special regard to flutter echoes. Furthermore, simulations in *CATT-Acoustic* of both the current state of the building and improvement measures will be performed.

To begin with, a general introduction to room acoustics including the theoretical fundamentals of the topic is provided in chapter 2.

Chapter 3 deals with the different measurement techniques that are used in room acoustics. This chapter serves as a preparation for the measurements described in the following chapter.

The purpose of the measurements performed in chapter 4 is to evaluate the general acoustical situation in the building on the one hand, and on the other hand to examine the flutter echoes in detail. In this section, first, an overview over the measurement object is given, followed by a description of the measurement setup/procedure.

The measurement results are presented and discussed in chapter 5.

In chapter 6, a simulation of the building is created. After a comparison between the model and the measurement results, different strategies against flutter echoes are described and reviewed by simulations.

The last chapter contains a summary of this thesis and a discussion of the results.

2 Theoretical Background

In this chapter, the theoretical fundamentals are presented that the following chapters build on, starting with the characteristics of sound. After a description of the three basic approaches to room acoustics, which are wave theory acoustics, statistical acoustics and geometrical acoustics, the phenomenon of echoes is explained.

2.1 Sound

Sound is a pressure fluctuation that can be perceived with the sense of hearing. From the view of physics, it can be described as particle vibrations in an elastic medium (typically air). Sound propagates as a longitudinal wave, which means that the particles oscillate in the direction of propagation. This is illustrated in figure 2.1, where a plane wave moves through an elastic surface that is excited by piston strokes. The elongation of groups of three molecules is shown schematically for 20 points in time (vertical axis). The horizontal curves illustrate the pressure distribution, which is used most time to visualize sound wave phenomena.

The frequency of sound approximately correlates with the sensation of pitch. A large frequency range from about 16 Hz up to 20 kHz is covered by the human hearing as well as a high dynamic range of more than 100 Pa, while the hearing threshold at 1 kHz is at a pressure of only 20 μPa. This is why often the sound level in dB referring to a reference value of $p_0 = 20\,\mu\text{Pa}$ is used instead of absolute values.

$$L_p = 20 \log \frac{p}{p_0}$$

In air, the velocity of sound c (not to be confused with the sound particle velocity v) is about 343 $\frac{m}{s}$ at 20 °C. In ideal gases, it only depends on temperature and increases with rising temperature.

2.2 Impulse Response

From the signal processing point of view, a room can be treated as a black box with an input $x(t)$ (sound source) and an output $y(t)$ (receiver, e.g. listener, microphone). This system can be fully described by its impulse response $h(t)$, which is the signal that would appear on the output with an ideal impulse $\delta(t)$ on the input for the current system configuration (see figure 2.2).

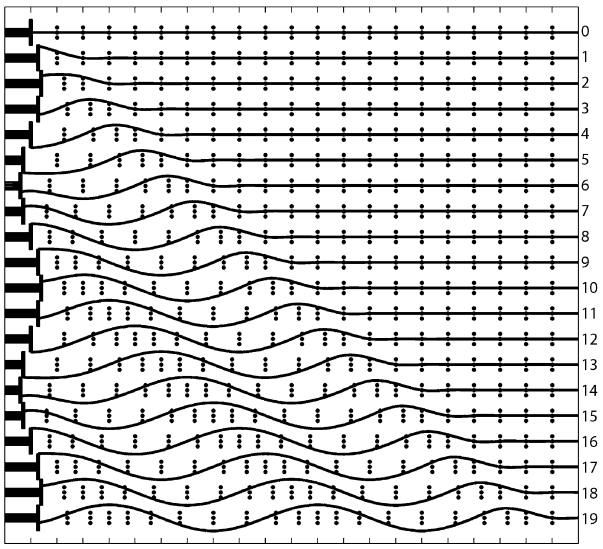

Figure 2.1: Propagation of longitudinal waves and pressure distribution [1, p. 19]

The fourier transform of the impulse response is the transfer function, which provides information of the influence of the transmission path on frequency and phase of the transferred signal.

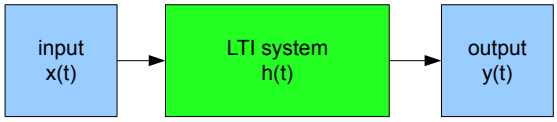

Figure 2.2: The connection between input and output of a system is its impulse response

In a simple room model for example, one would see a strong direct sound impulse at the time corresponding to the distance between source and receiver and, later, the pulses thrown back from reflective surfaces, appearing at the respective travel time they need to reach the receiver, scaled in amplitude and phase depending on the absorption parameters of the surface and the air absorption. Except for the very first reflections from the closest surfaces, it is mostly impossible to distinguish single reflections in the impulse response in real-world rooms. The reason for this is the great density of reflections and the development of a diffuse sound field. Instead, the acoustician often looks at other measures that can be calculated from the impulse response, like energy ratios, frequency content or, most important, the reverberation time.

2.3 Wave Theory Acoustics

Wave theory acoustics is the fundamental physical-mathematical concept of describing a sound field by the solution of the wave equations. As it can only be applied to simple-geometry rooms, it is used to describe the basic sound phenomena of propagation, reflection, absorption, diffraction, superposition of waves as well as the sound impedance [2, p. 3].

An important use of wave theory is often to determine the resonances of a room. Assuming ideal sound-hard parallel walls at a distance, which is an integral multiple of half of a wavelength, the reflected wave is in phase with the incident one and interferes constructively. The

resulting stationary sound field is called a *standing wave*, its frequency is an *eigenfrequency* or *natural frequency* of the room. It is characteristic that nodes, where sound pressure is zero, and antinodes, where the oscillation has the highest amplitude, develop at fixed positions. Figure 2.3 illustrates this with two standing waves of different frequency.

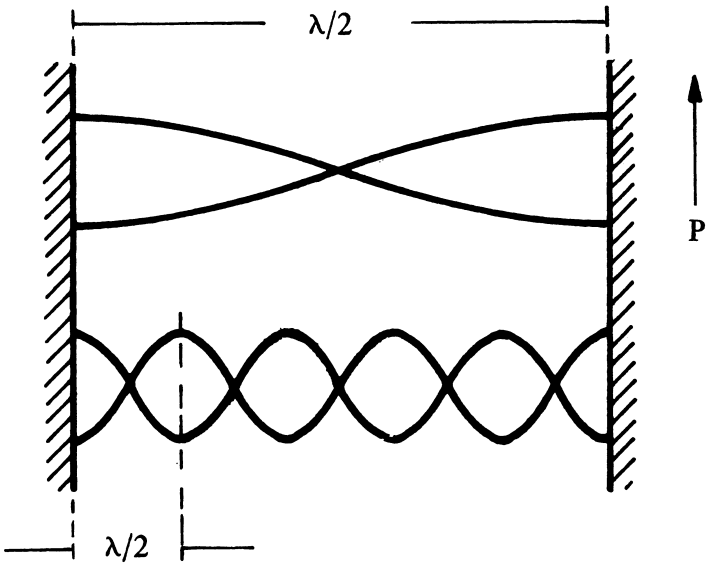

Figure 2.3: Sound pressure distribution of standing waves [3, p. 10]

If the wave propagates in all three dimensions, a sound interference pattern develops. It is called *eigenmode*, if also stationary nodes and antinodes can be observed (see [4, p. 10]).

In a rectangular room with sound-hard walls with the physical dimensions $l_x \times l_y \times l_z$ like shown in figure 2.4, the eigenmodes can be calculated by the solution of the wave equation. The mode frequency f_r is determined by the three integer ordinal numbers n_x, n_y and n_z. These values are the number of node planes in the respective direction. Figure 2.5 visualizes the natural frequencies in frequency space. Each point of the grid corresponds to a certain eigenfrequency which is equal to the distance of the respective point to the coordinate origin:

$$f_r = |\vec{f_r}| = \frac{c}{2}\sqrt{\left(\frac{n_x}{l_x}\right)^2 + \left(\frac{n_y}{l_y}\right)^2 + \left(\frac{n_z}{l_z}\right)^2} \tag{2.1}$$

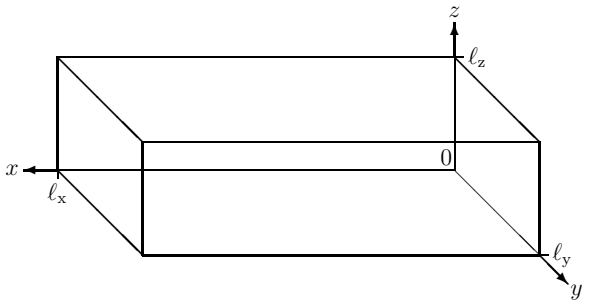

Figure 2.4: Rectangular room and coordinate system [5, p. 216]

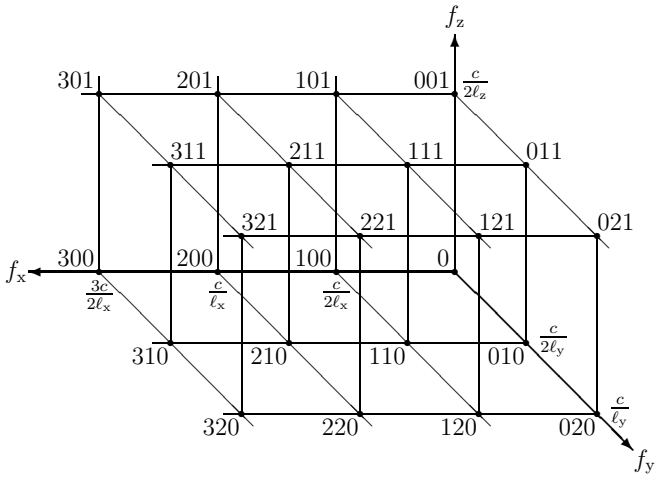

Figure 2.5: Natural oscillations in frequency space [5, p. 217]

One speaks of *resonant frequencies* or *room modes* if a sound source is introduced at a certain position of the room. Depending not only on its frequency content, but also on the source position, it will excite certain room modes more or less strongly. Room modes usually are perceived as disturbing because they cause level increases at the respective frequencies (see [4, p. 13]), and avoiding them is a major task of room acoustics.

As you can see in figure 2.4, the number of eigenmodes is increasing quickly if frequency rises. If a certain frequency is exceeded, the density of the modes at each semitone is so high that they are not perceived as resonances anymore. This limit frequency which is also called *Schröder Frequency*.

In ordinary rooms, it only depends on the room volume V and the reverberation time T:

$$f_c \approx 2000 \sqrt{\frac{T}{V}} \text{ [Hz]} \tag{2.2}$$

In large spaces, often room modes are of minor importance: because of the large volume, the mode density is already quite high at low frequencies. But in a narrow hallway, which might have also a large volume, the mode density in one dimension might be lower, which leads to perceivable resonances.

2.4 Statistical Acoustics

If the room geometry is too complicated for using wave theory acoustics, which is in the majority of cases, and if it is not sufficient to track a relatively small number of sound rays over short time intervals like done in geometrical acoustics, statistical considerations help to provide a good overall view of the acoustic characteristics. *Statistical acoustics* looks at the temporal distribution of sound energy between sources and sinks (e.g. absorbers). It is only applicable under diffuse field conditions, assuming that the energy density is evenly distributed in space (see [2, p. 62]).

The *reverberation radius* defines the border between direct and diffuse field as the radius where the direct sound level equals the level of diffuse sound in the room. The difference between direct field and diffuse field is that in the direct field, sound comes from one ore more certain directions (sources or reflectors), while in a diffuse field sound incident from any direction is equally probable (see [3, p. 20]).

Figure 2.6(a) illustrates the basic concept of statistical acoustics. It shows a water container with an inflow of water on the top and a drainage surface at the bottom. The inflow stands for an acoustic source and the drain symbolizes the conversion of sound energy into other forms of energy (absorbent surfaces and air absorption). The room is filled with sound energy from the source until a state of equilibrium is obtained. After turning off the source, sound energy will "drain off" in a certain time, which is called reverberation.

In figure 2.6(b), you can see the time curve of the (diffuse field) sound pressure level for a direct sound level with rectangular envelope. It shows a certain attack slope after turning on the source and a decay after turning it off, corresponding to the model in figure 2.6(a).

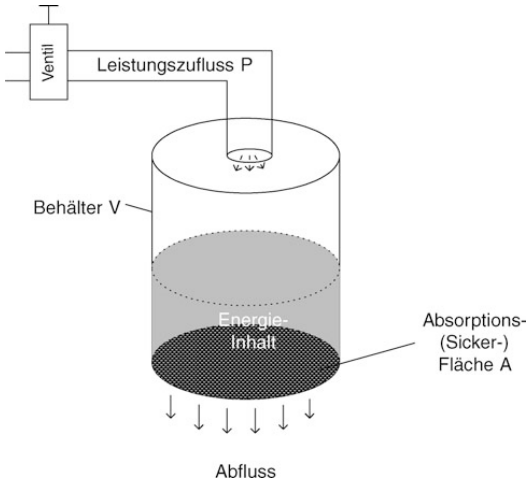

(a) Analogy between a leaking container and the sound energy content of a room. *[6, p. 232]*

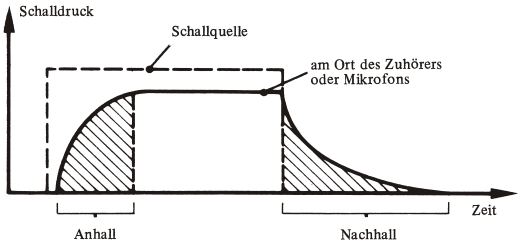

(b) Typical sound energy characteristic. *[3, p. 21]*

Figure 2.6: Sound energy in statistical acoustics

Reverberation

At the beginning of the 20th century, the American physicist Wallace C. Sabine showed experimentally that the length of the reverberation in a room is independent from the sound signal as well as the excitation level. He showed that the duration of audible reverberation was a unique feature of a room, using only simple equipment (organ pipes, a stopwatch and his ears) [7, p. 146].

Even if todays measuring techniques are more advanced, the reverberation time stayed the central parameter in architectural acoustics and many of the assumptions made more than 100 years ago were proved to be correct.

Because the reverberation decays exponentially, the logarithmic decay can be approximated by a straight line. This includes short sound pulses as well as orchestra music, as you can see in figure 2.7.

Reverberation Time

In general, the *reverberation time* is considered as the duration of audible reverberation under optimal conditions. Since the maximum dynamic range of the human hearing covers about 60 dB for fast level changes, the term reverberation time (T_{60}) refers to the time until the sound energy level has fallen by 60 dB compared to the initial sound energy level. This means that the sound pressure has fallen by a factor of 1000.
Mostly, it is impossible to measure the decay over a range of 60 dB because it is limited by the background noise level and the distortion-free excitation level, especially over larger distances.

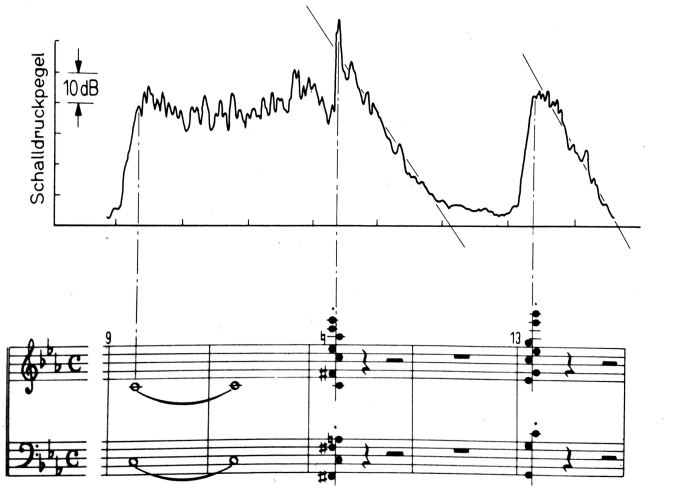

Figure 2.7: Level decay during an orchestra concert [7, p. 149]

It is hence common to measure the time needed for a decay of 30 dB or 20 dB and extrapolate the results to 60 dB (T_{30}, T_{20}).

Figure 2.8 shows the process of a simple reverberation time measurement. After excitation of a room with, for example, white noise, the source is turned off after a while. The recorded system response passes through a filter bank and and a straight line is fitted to the decay curve, from which the reverberation time can be read off. Typically, it is averaged over several measurements at different positions in the room.

In a T_{30} measurement, the reverberation time is usually read off from -5 dB to -35 dB because the slope of the early decay is often different from the rest of the curve. However, this *early decay time*, which is actually the duration of a decay over the first 10 dB, extrapolated to - 60 dB, often determines the subjective impression of the reverberation.
The reverberation time is proportional to the volume V and inversely proportional to the total

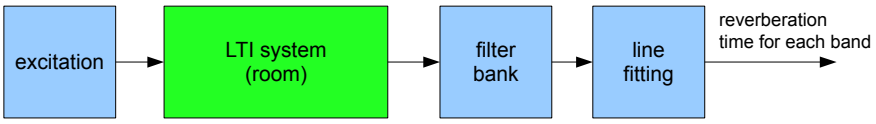

Figure 2.8: Reverberation time measurement (simplified)

equivalent sound absorption area A_{tot}, which is the area with an absorption coefficient α of 1 (total absorbent) that can be calculated by adding up the products of each partial surface S_i of the room and its mean absorbance $\alpha_{m,i}$:

$$A_{tot} = \sum_{i=1}^{n} \alpha_{m,i} \cdot S_i \tag{2.3}$$

The empirically determined formula for the reverberation time by Sabine is:

$$T = 0.161 \frac{\mathrm{s}}{\mathrm{m}} \cdot \frac{V}{A_{tot}} \tag{2.4}$$

This statistic formula only delivers reliable results if the absorption is evenly distributed, and if the room geometry is not too complex (see section 6).

2.5 Geometrical Acoustics

Although sound is a pure wave phenomenon, sometimes it makes sense to describe it by a model of sound rays that propagate in a certain direction carrying a certain amount of energy. This model is called *geometrical acoustics*. This approach is able to explain sound reflection and acoustic shadowing in a simple way, which is useful since wave theory can hardly be applied on real, complex rooms. The wave phenomena diffraction and refraction mark the limits of the applicability of geometrical acoustics [2, p. 78].

Figure 2.9 illustrates acoustic shadowing with obstacles of varying size. It shows, that if the object dimensions are in the same area as the wavelength, the sound waves are bent around the obstacle. Only if the wavelength is larger than the obstacle dimensions, shadowing takes place (neglecting transmission). Geometrical acoustics only considers this wavelength range.

In case of broad-band sound, the higher frequency components will be reflected and the lower components will be bent around the obstacle. The application of *mirror sound sources* even

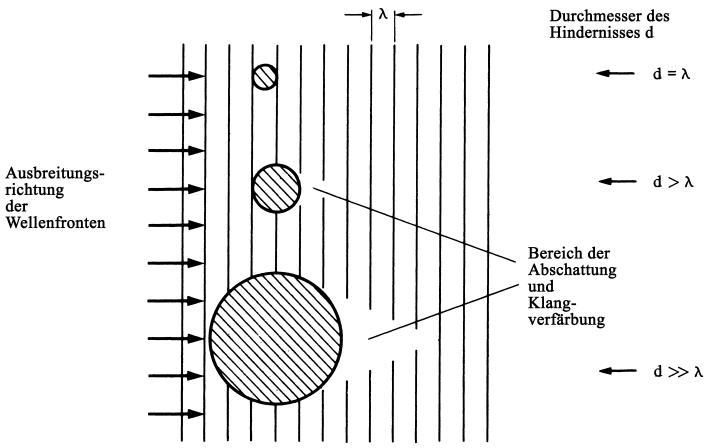

Figure 2.9: Acoustic shadowing, variable obstacle size. [3, p. 13]

allows to estimate direction, level and travel time of early reflections based on geometrical construction. Figure 2.10 shows the first and second order mirror sources between two parallel walls. Based on the length of the arrow pointing away from the original source S_0, which indicates the time passed after emission of a cylindrical wave (2-dimensional case), the position of the wave front around the source and its reflections, caused by S_1 and S_1', and are geometrically constructed (upper picture). This procedure can be repeated many times (lower picture), but it quickly becomes confusing. Better results are provided by acoustics simulation software using sound ray tracing, like *CATT-Acoustics*, which will also be used for the simulations in this thesis.

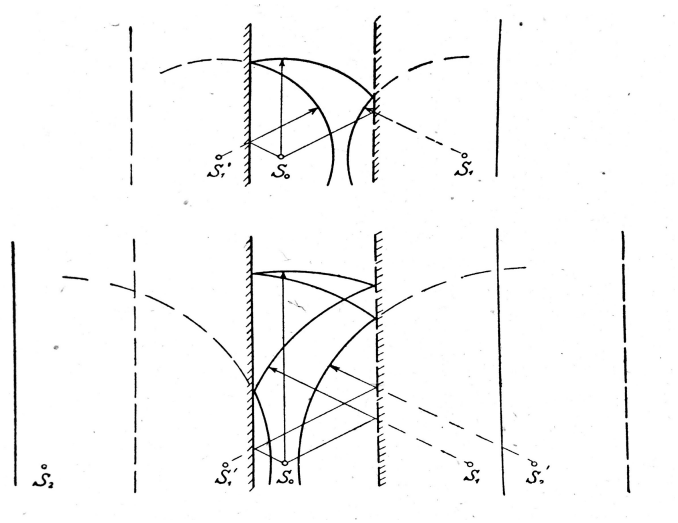

Figure 2.10: Geometrical construction of reflections using mirror sources [8, p. 18]

2.6 Echo

In this thesis, an *echo* will be referred to as a sound reflection, which is perceived as a repetition of the original sound [8, p. 54]. If not intentionally used as an effect, echoes are mostly perceived as disturbing and should therefore be prevented.

For the perceptibility of echoes, it is crucial that the respective reflection is not affected by *temporal masking*. This means that the time interval between the arrival of the direct sound and the arrival of the reflection must exceed a certain limit that also depends, among other things, on the level and the character of the sound (e.g. impulsive/continuous, narrow-band/broad-band). Such high propagation times can be observed if there exist distant reflective surfaces, or if the sound is reflected multiple times before it arrives at the listener. The echo perception threshold is sometimes considered as 50 ms [2, p. 87]. Very early echoes that are rather perceived as coloration than as single sound events are used for orientation and spatial perception by the sense of hearing.

Flutter Echo

The term *flutter echo* characterizes a special case of an echo that often occurs between two parallel surfaces consisting of weakly sound-absorbing material, placed in a certain distance from one another.

A flutter echo can be described as a "transient vibration excited by an impulsive sound" [9, p. 173], for example clapping hands or footsteps. Its distinctive feature is the fluttering sound that comes from the periodic repetition of the original pulse. Between distant walls, one has the experience of hearing a series of pulses [9, pp. 170 f.]. But if the walls are close together, it is not perceived as a series of pulses anymore and the flutter echo has a tonal character. Its fundamental period is equivalent to the time difference between the pulses that arrive at the listener [8, p. 60].

Physically, flutter echoes can be viewed as an one-dimensional spatial oscillation of sound energy with decreasing amplitude due to the conversion into thermal energy (friction loss) at absorbing surfaces and the air absorption between them.

A mathematical description of the flutter echo between two sound-hard walls was given by Dah-You Maa in 1941 [9], based on the homogenous wave equation for free vibrations. He also described the directional effect of flutter echoes. Between two parallel walls, the echo always

seems to come from the wall that is further away from the listener, even if it is a countinuous sound.

A simulation was performed to illustrate the phenomenon. Figure 2.11 shows the sound pressure between two infinitely rigid walls at $x = 0\,\mathrm{m}$ and $x = 10\,\mathrm{m}$, based on the derivations in [9], if a sound source at $x = 2\,\mathrm{m}$ sends out one wave packet each in positive and negative x direction at time zero.

Note that the position x is plotted on the vertical axis. As time passes, the wave packets travel between the walls, interfering wherever they hit each other, and the listener, assumed to be at the source position indicated by a blue line, will have the impression of hearing a flutter echo caused by the pulses that are heard, every time a wave packet crosses the blue line.

One can easily observe that the longest break between the arriving wave pulses takes place, before "new" pulses arrive from the wall at $x = 10\,\mathrm{m}$. According to the *precedence effect*, especially if no level differences exist, the directional impression is determined by the first wave front arriving at the listener, which in this case comes from the wall which is further away.

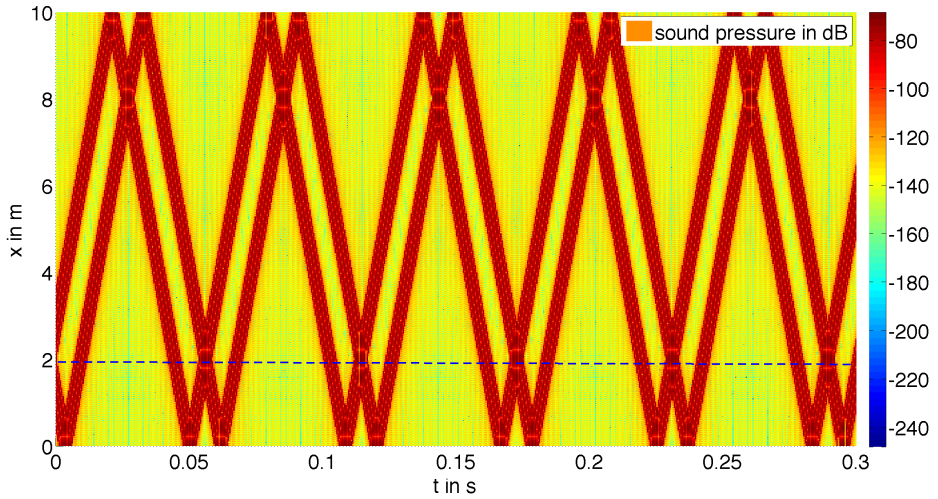

Figure 2.11: Flutter echo: Simulation of the sound pressure over time between infinitely rigid walls. The dashed line corresponds to the position of the sound source.

3 Measurements in Room Acoustics

The most common purpose of measurements in room acoustics is to examine the acoustical behavior of an enclosure in order to evaluate its acoustic qualities with regard to the respective type of use. There are different techniques that can provide various information about the room. For measuring the reverberation time, one can determine the decay curves directly, or use more advanced (indirect) techniques like measuring the impulse response of the system. The decay curve can be computed out of the impulse response, together with a variety of other system characteristics. These modern techniques offer various advantages compared to the direct methods, which will be described and compared in the following section in order to find the optimal solution for the measurements that will be performed in the course of this thesis.

3.1 Measurement Methods

3.1.1 Impulse Excitation Method

The most simple way of measuring the reverberation time is to excite the room with a sound impulse. This method should not be confused with measuring the impulse response which is is defined as the output signal for an ideal impulse at the input of a system. The impulse excitation method provides only an approximation of the impulse response, caused by the fact that one can not generate an ideal impulse which (in our continuous environment) would have infinite amplitude while being infinitely short.

Because in a simple physical room (approximately linear and time-invariant), the slope of the logarithmic decay curve of any sound is constant [2, p. 66], one could theoretically use any signal to determine the reverberation time. The advantage of using impulsive sound is the simplicity of the measurement setup and thus the possibility of generating high sound pressure levels (resulting in a better signal-to-noise ratio) without the risk of producing a distorted excitation signal; instead of employing electro-acoustical sources, one can use gunshots or electrical spark gaps for sound generation [10, p. 173].

The block diagram below (figure 3.1) illustrates a possible measurement setup of the impulse excitation method. The system response to a sound impulse is recorded and divided into octave bands or 1/3-octave bands by a filter bank Then a regression line is fit to the decay of each band, which allows to read off the reverberation time, as explained in chapter 2.

Although this method allows to generate very high sound pressure levels, the signal-to-noise ratio that can be gained with impulsive sound is relatively low, considering that in the short

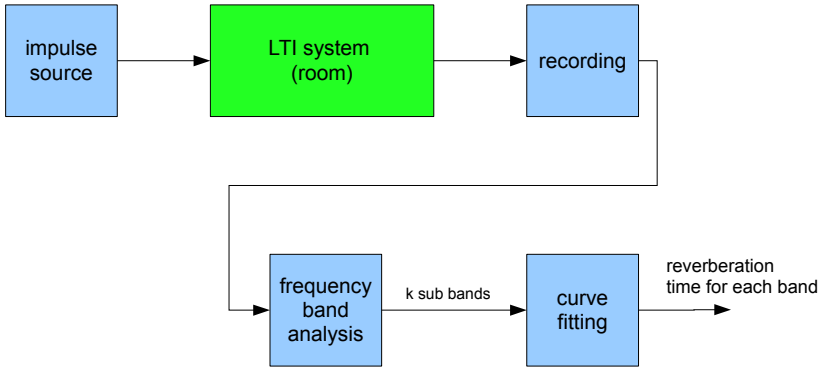

Figure 3.1: Impulse excitation method: possible measurement setup

duration of the impulse only a small amount of energy can be fed into the enclosure.

3.1.2 Interrupted Noise Method

In contrast to the method described in section 3.1.1, the signal used here is of continuous kind, provided by a broad-band noise source. Often pink noise is used, which leads to a uniform energy distribution after octave-band filtering. Also, it makes sense to increase the SNR at low frequencies, since the noise floor in common rooms tends to be most present in the low frequency range [11, p. 12] and because the pitch resolution of the human hearing decreases with frequency.

Unlike with the impulse method, the sound source is left turned on for a while in order to fill the room with sound energy and thus to obtain stationary conditions [12, p. 207], which means balance between "inflowing" (source) and "draining off" (absorption) sound energy [5, p. 232]. This is illustrated in figure 2.6(a).

As recommended by *ISO 3382-2*, the source is turned off after a sufficient period of time of at least half the reverberation time (several seconds in large enclosures). Figure 3.2 shows an example of a decay curve, where L_0 is the stationary sound level and L_N is the noise level.

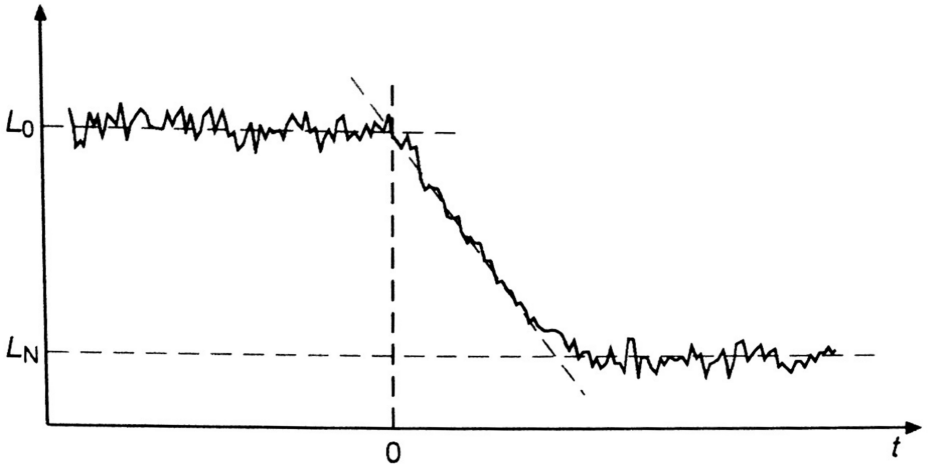

Figure 3.2: Decay after turning off the source [11, p. 7]

Due to the stochastic character of the excitation signal, it is necessary to average over multiple measurements at each microphone position [13, p. 10]. One can either calculate the mean of the determined reverberation times for each decay curve, or average over the measured squared decay curves.

A possible measurement setup is shown in fig. 3.3.

The standard deviation σ allows an estimation of the measuring uncertainty for the interrupted noise method:

$$\sigma(T_{30}) = 0.55 \cdot T_{30} \sqrt{\frac{1 + \frac{1.52}{n}}{N\,B\,T_{30}}} \tag{3.1}$$

In the equation above, n is the averaging number of decays at each position, B is the bandwidth of the regarded octave band which is equivalent to $0.71 \cdot f_c$, where f_c is the respective center frequency. N represents the number of independent measurement points and T_{30} is the reverberation time for an observed range of 30 dB [13, p. 12]. For example, if measuring T_{30} at the 1 kHz band using 3 microphone positions and double averaging for each, the standard deviation will be $\sigma \approx 20\,\text{ms}$, assuming a reverberation time of $T_{30} = 1.5\,\text{s}$.

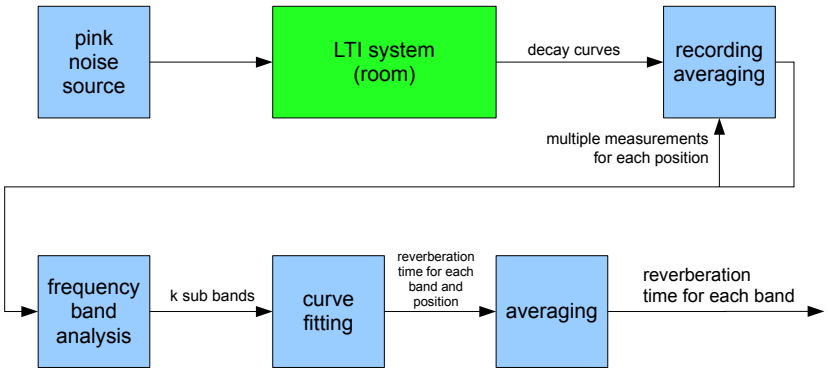

Figure 3.3: Interrupted noise method: possible measurement setup

3.1.3 Sine Sweep Excitation

As mentioned before, the impulse response of a system is the response to the excitation by an ideal impulse with a white spectrum. The following method for measuring the impulse response takes advantage of the fact, that an ideal impulse and an ideal sine sweep share the same spectral content.

From the perspective of signal processing, what a listener will hear if sound is played back in a room can be described as the convolution of impulse response of the room and the original sound, neglecting the transfer functions of the playback and recording equipment. Hence, the main idea of using sine sweeps for system identification is to deconvolve the output signal and the known original signal in order to calculate the impulse response.

A sine sweep with linear increasing circular frequency ω (see fig. 3.5(a)) can be written as:

$$x(t) = \sin \varphi(t) \qquad \varphi(t) = \int \omega(t) \mathrm{d}t \tag{3.2}$$

Assuming a linear and time-invariant system, the output signal, which is the result of the convolution of the sweep signal x and the inpulse response h

$$y(t) = (x * h)(t) \tag{3.3}$$

can also be written in frequency domain as the product of the fourier transform of x and the transfer function H:

$$Y(j\omega) = X(j\omega) \cdot H(j\omega) \tag{3.4}$$

Therefore the transfer function can be determined by spectral division

$$H(j\omega) = \mathcal{F}\{h(t)\} = \frac{Y(j\omega)}{X(j\omega)} \tag{3.5}$$

The impulse response can therefore be obtained by applying the inverse fourier transform on the above expression, resulting in the expression

$$h(t) = \left(\mathcal{F}^{-1}\{\frac{1}{X}\} * y\right)(t) \tag{3.6}$$

which is the convolution of the output signal and the inverse fourier transform of $X^{-1}(j\omega)$ that is equivalent to the time reversed input signal [14, p. 120].

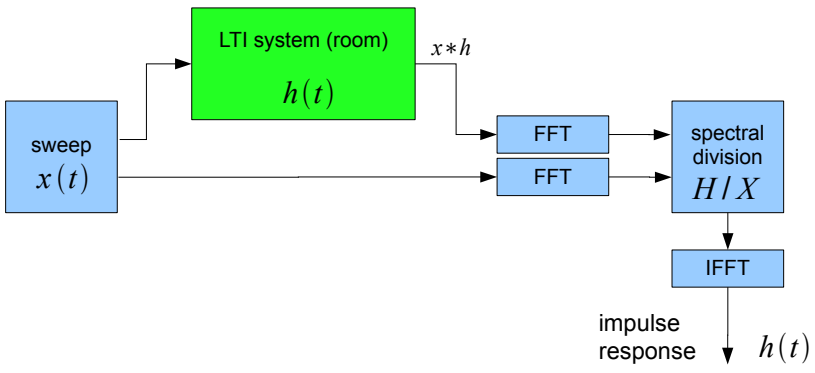

Figure 3.4: Measurement of impulse response with a sine sweep

As already mentioned in section 3.1.2, both the background noise and the frequency resolution

of the human hearing decrease with rising frequency. It is therefore beneficial to put a higher amount of energy into the lower frequency range in order to enhance the signal-to-noise ratio in the relevant spectral region. This can be accomplished by using sweeps with exponentially increasing frequency with time (see fig. 3.5(b)) that have a pink spectrum [14, p. 109]: its power spectral density decreases with frequency.

Unlike if using linear sweeps, the amplitude of the inverse signal for deconvolution must be weighted to compensate the non-uniform energy distribution [14, p. 120] to get an unfiltered impulse response.

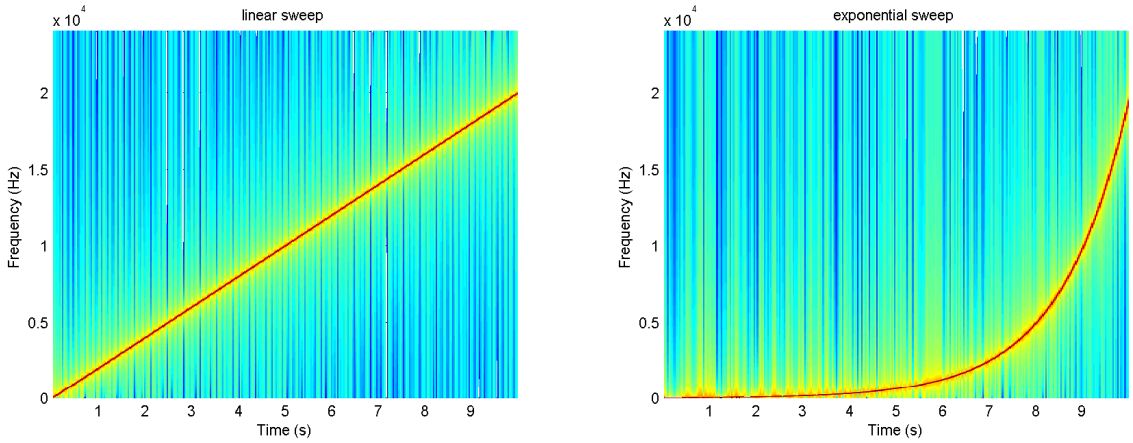

(a) linear sweep

(b) exponential sweep

Figure 3.5: Spectrograms of linear and exponential sweep

The signal-to-noise ratio that can be achieved with the swept sine method depends on various parameters. It increases by 3 dB when doubling the sweep duration. Further parameters are the sweep rate and the excitation level [11, p. 29] and the environmental noise. One advantage is the possibility of excluding all harmonic distortion products from of the resulting impulse response. This is achieved by time-windowing of the raw impulse response as the distortion components appear at negative times [15, p. 453] before the "arrival" of the direct sound impulse.

3.1.4 Maximum Length Sequences

In the previous section it was shown how it is possible to obtain impulse responses from the convolution with a sine sweep by spectral division. Now another approach will be described that applies the correlation function on excitation signals called *Maximum Length Sequences* (MLS) in order to calculate the room impulse response. The MLS is a periodic binary pseudo-random noise signal. *Pseudo-random* means that the signal is deterministic (fully predictable and reproducible), but it is uncorrelated and has therefore similar spectral properties as white noise [16, p. 4].

The *cross-correlation* shows relations between two different signals. Analogous, the *autocorrelation*, which is the cross-correlation of a signal with itself, is a measure for the inner statistical relations of a signal and can reveal stochastic or periodic components. The definition of the autocorrelation function of a real, causal (right-sided) continuous signal $x(t)$is

$$\Phi_{xx}(\tau) = \big(x \star x\big)(\tau) = \lim_{T\to\infty} \frac{1}{T} \cdot \int_{n=0}^{T} x(t) \cdot x(t-\tau)\mathrm{d}t \tag{3.7}$$

Since the processing takes place in the digital domain after A/D conversion, the following considerations will be made for discrete-time signals.

The autocorrelation sequence $\Phi_{xx}[n]$ of an ideal random sequence always has a peak at a shift of zero that corresponds to the mean power σ_x of the signal (the mean square of x), and is zero elsewhere, as it is fully decorrelated. [17, p. 186 ff.]. Therefore it can be expressed as a weighted unit impulse δ :

$$\Phi_{xx}[n] = \delta[n] \cdot \sigma_x$$

For periodic noise, such as the MLS which has a period of $L = 2^m - 1$ samples (the MLS length), the signal correlates with itself each period and the expression becomes

$$\Phi'_{xx}[n] = \begin{cases} 1, & n = kL \\ -\frac{1}{L}, & n \neq kL \end{cases}, \; k \in \mathbb{Z}, \; n \in [-L, L], \tag{3.8}$$

where the $'$ indicates the periodicity of Φ'_{xx}. For large L, the offset of $-\frac{1}{L}$ approaches zero and the auto-correlation, which is only 1 at kL, equals the periodic pulse $\delta'[n]$ [14, p. 104].

This very property can be utilized for system identification. If a system is excited with an MLS signal $x'[n]$ at the input, the output $y'[n]$ will be the convolution of the pseudo-random sequence and, in our case, the room impulse response:

$$y'[n] = \big(x' * h\big)[n]. \tag{3.9}$$

We can apply the cross-correlation on this equation and the original MLS sequence and thereby receive

$$\begin{aligned} \Phi'_{xy}[n] &= \big(x' \star y'\big)[n] \\ &= \big(x' \star (x' * h)\big)[n] \\ &= \big((x' \star x') * h\big)[n] \\ &= (\Phi'_{xx} * h)[n] \end{aligned} \tag{3.10}$$

which is the convolution of the well-known autocorrelation of x and the impulse response. Using the relationship from (3.8), the result is the convolution of the impulse response and the periodic δ-pulse (and the DC offset of $-\frac{1}{L}$):

$$\Phi'_{xy}[n] \approx \big((\delta' - \frac{1}{L}) * h\big)[n] = h'[n] - \frac{1}{L}\sum_{k=0}^{L-1} h'[k] \approx h'[n], \;\; L >> 1 \tag{3.11}$$

The convolution of an arbitrary signal and an impulse $\delta[n-\xi]$ shifts the signal by the offset ξ and, if the pulse is periodic, the result will have the same period as the pulse. Therefore the cross-correlation of the MLS signal and the system response is approximately the periodic impulse response $h'[n]$ (see fig. 3.6)and a DC offset that can be neglected for large L (see [14, p. 107]).

3.2 Calculation of the Decay Curve

Since the impulse response fully characterizes the room, it does not take great effort to estimate its associated decay curve. The basic procedure was introduced by Schroeder in 1965 [18] and is part of *ISO 3382* [19, p. 11 f.]. The following description is based on this standard.

The estimation procedure of the sound energy decay curve $E(t)$ is often referred to as *Schroeder-backwards integration*. Assuming ideal conditions, it is the integral from infinity to t of the squared sound pressure of the impulse response

$$E(t) = \int_t^\infty p^2(\tau)\mathrm{d}\tau \tag{3.12}$$

which can be rearranged to

$$E(t) = \int_0^\infty p^2(\tau)\mathrm{d}\tau - \int_0^t p^2(\tau)\mathrm{d}\tau\,. \tag{3.13}$$

For real impulse responses with non-zero SNR the integral may be calculated from the intersection point t_1 between the noise floor level and the linear envelope of the logarithmic squared sound pressure decay of the impulse response, in order to minimize the influence of noise to the energy decay curve:

$$E(t) = \int_t^{t_1} p^2(\tau)\mathrm{d}\tau + C\,,\ t < t_1\,. \tag{3.14}$$

C is a correction term to prevent systematic underestimation of the reverberation time resulting from the finite integral. The standard specifies that for a maximum underestimation of 5 % the SNR_{dB} of the impulse response has to be at least 15 dB plus the evaluation range (in total 45 dB for T_{30}).

A major benefit of the impulse response method is that a decay curve estimated from a single room impulse response is identical with the average decay curve of infinitely many interrupted-noise measurements [13, p. 11]. That means that one only has to do spatial averaging but not averaging of several measurements at one measuring position.

In figure 3.7 the different stages of the calculation process are illustrated by a measured impulse response (fig. 3.7(a)), the squared sound pressure level (fig. 3.7(b)) and the energy decay level (fig. 3.7(c)). The curves are normalized to 1 respectively 0 dB.

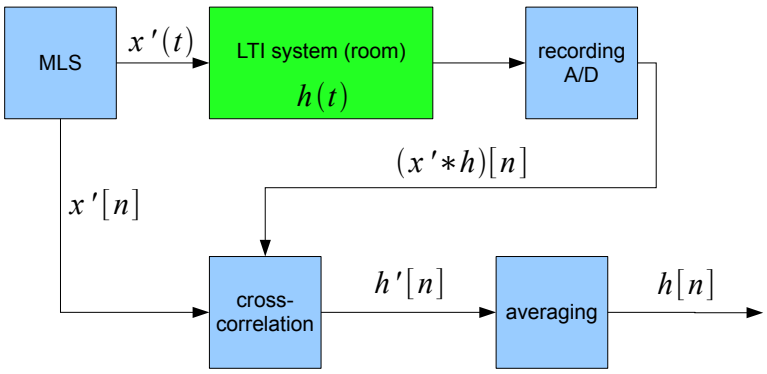

Figure 3.6: Impulse response measurement with MLS

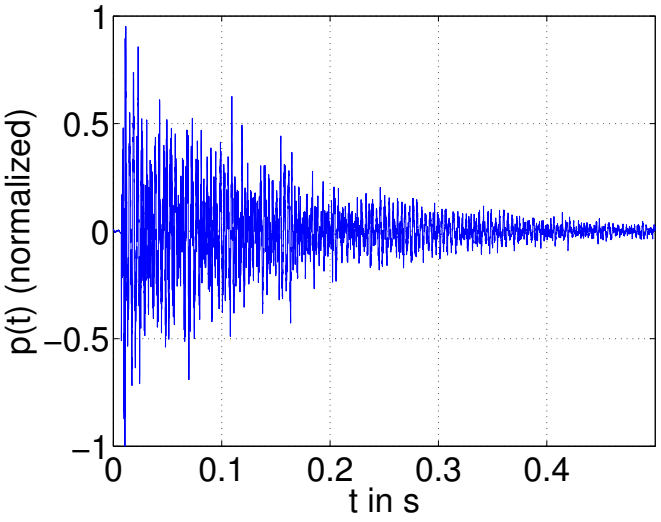

(a) impulse response

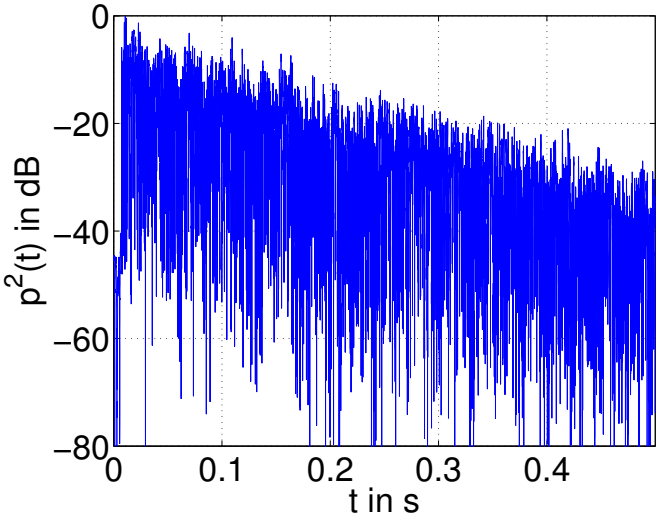

(b) squared impulse response

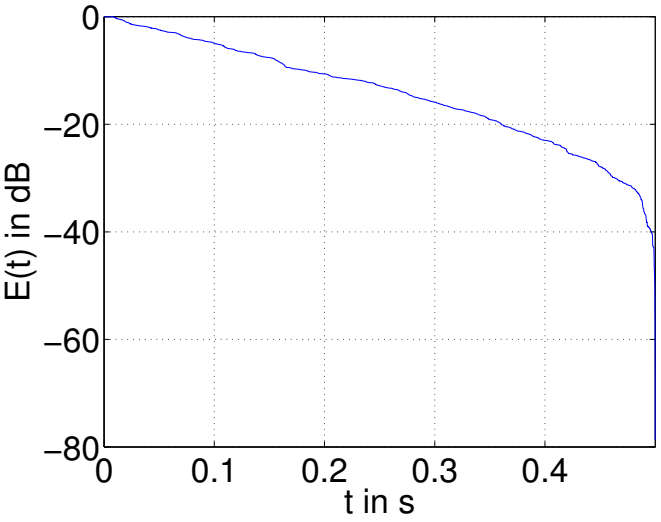

(c) energy decay

Figure 3.7: Estimation of decay curve

3.3 Conclusion

In the previous sections, several measurement methods in acoustics were presented. In order to decide, which one to chose, a short comparison will be made in the following.

All of the strategies can be used to measure the reverberation time. A reverberation measurement is the minimum requirement for acoustic evaluation of a room, but it may not be sufficient if the appearance of echoes is to be examined. The question is why not to take advantage of the additional information the "modern" methods provide. Of course, the implementation of the "classical" methods seems to be easier, especially the impulse excitation method allows to use highly mobile equipment in form of hand-held devices.

But since accuracy is more important than mobility, the signal-to-noise ratio has to be considered. It can be difficult do gain a sufficient SNR with the "classical" methods and the building, which will be examined, is quite large. Therefore either sweeps or MLS should be used. An additional advantage of these methods is that they don't require averaging at each measurement point like the interrupted noise method does.

One advantage of the swept-sine method is that very high SNR values can be gained. This is why sweeps are the best solution for high-quality auralization purposes [15, p. 469]. On the other hand, the possible SNR the MLS method is able to provide is expected to be sufficient. Using MLS could also be advantageous because of the ability to suppress sound, which is uncorrelated with the excitation signal, as it can possibly occur by ticking clocks and the drink dispensers in the building, as well as the persons who are present during the measurement.

Based on this consideration the MLS method was used for the following measurements.

4 Performance of Measurements

The geometrical properties and the acoustics of the building 16 c will be described in this chapter. Furthermore, the measurement setup is explained in detail.

4.1 Measuring Object

The examined enclosure is a hallway in the building Inffeldgasse 16 c, Graz. It is part of an architectural complex of eight similar three-story university buildings finished in 2001 (fig. 4.2). The appearance of the architectural award-winning building is dominated by orthogonal elements and the extensive use of concrete.

The internal space is more than 76 m long and between 10 m and 11 m high, while the narrowest parts of the corridor are only 2.9 m wide, which is a small distance compared to the overall length. The floor area of the ground floor is 354 m^2. Figure 4.1 shows the ground plan of building 16 c and the coordinate system, which was used also in the simulation. In the following, when referring to the left or right side of the building, viewing direction towards increasing y is assumed.

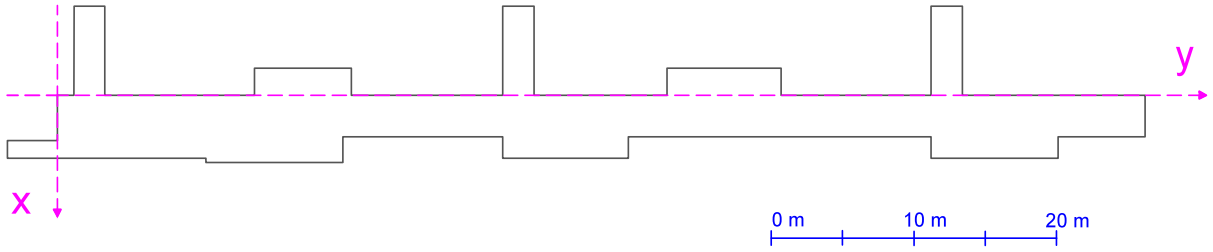

Figure 4.1: Ground plan of building 16 c

The interior free space is basically cuboid-formed and the volume (containing all connected side spaces) adds up to approximately 3750 m^3. The walls consist of raw, smooth and unpainted concrete with metal doors on both sides, interrupted by several windows and glass elements. Front and back side also consist of glass. The building has a concrete floor; the ceiling structure alternates between sky lights and lower elements with perforated metal cladding. Where the corridor differs from the 2.9 m minimum width (e.g. at the working spaces), the 2.67 m high ceiling is also revetted with perforated metal (also at the upper stories). Galleries in the upper stories are connected by bridges (see fig. 4.2(e)).

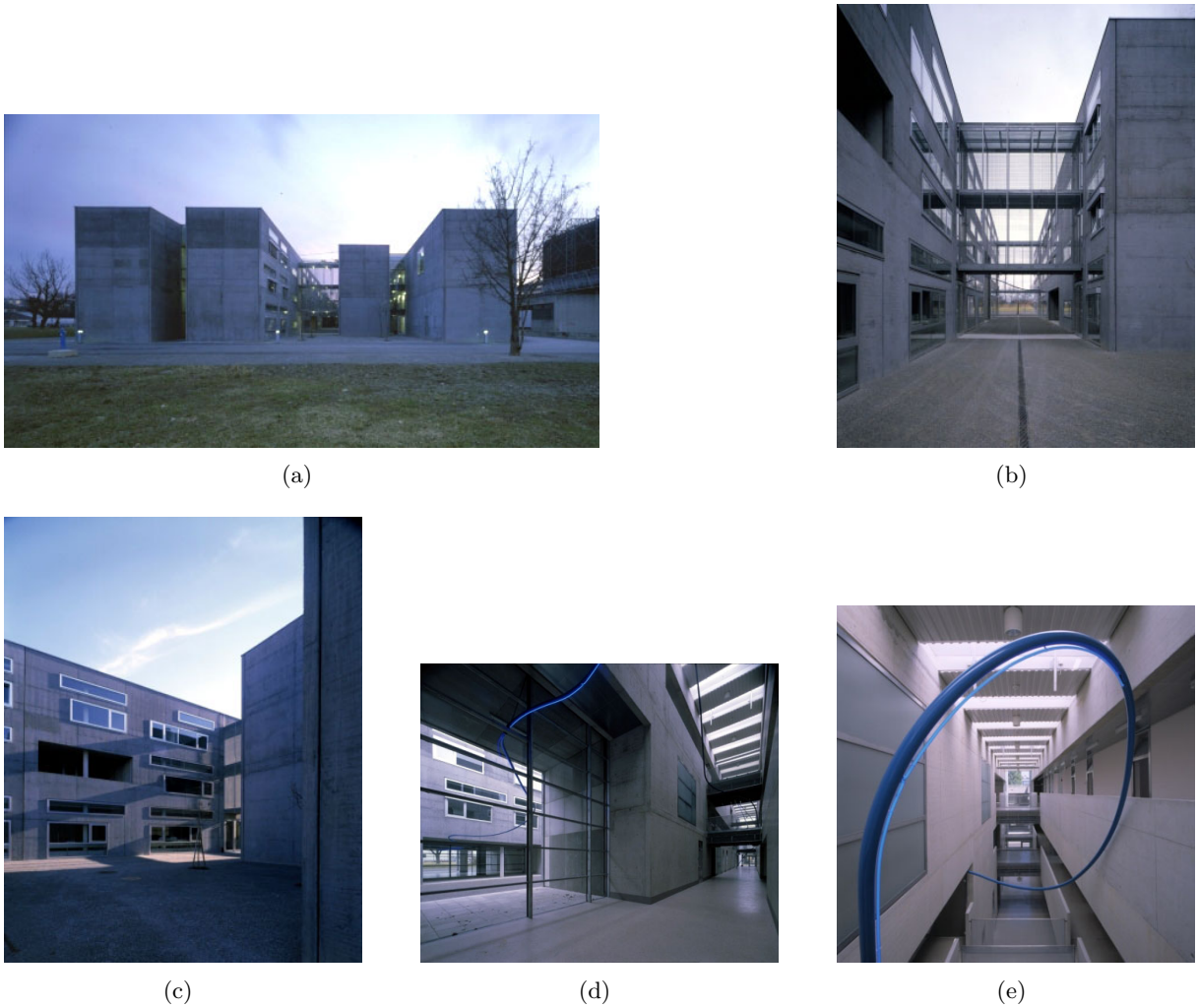

(a) (b)

(c) (d) (e)

Figure 4.2: Building complex Inffeldgasse 16. P. Ott, Riegler Riewe Architects Pty. Ltd., [Online], viewed: May 12, 2015, available: http://www.rieglerriewe.co.at/projects/ec_inff/0.html

Because the hallway is not only used as a passageway but also as lounge and working space, the acoustical properties of the enclosure are of high importance for speech intelligibility and working atmosphere and therefore must be considered in the architectural design process.

In this particular building, a flutter echo can be observed which can be heard most distinct at the narrow parts of the corridor (see hatched areas in fig. 4.3).

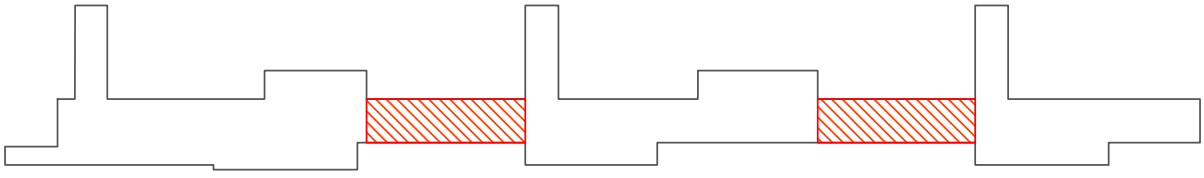

Figure 4.3: Areas with flutter echoes

4.2 Measurement Setup

The measurement pursues two main goals. First, the general acoustic situation needs to be examined through a measurement of the reverberation time and room acoustics parameters of the entire enclosure, which will be referred to as the *global* measurement in the following. Second, a detailed *local* measurement is performed in an area where flutter echoes occur.

Measuring equipment:

- *AKG C480* microphones and *AKG CK 62 ULS* omni-directional capsules
- *Fireface 800* audio interface
- *Norsonic Nor276* omni-directional sound source
- *Norsonic Nor280* power amplifier
- *testo 610* digital thermometer / hygrometer
- *Bosch DLE 70 Professional* laser rangefinder
- *WinMLS 2004* acoustic measurement software

An MLS signal with the following properties was used:

- order $m = 18$
- eightfold averaging
- 1 pre-send cycle
- MLS type A
- sampling frequency $f_s = 48\,\text{kHz}$
- total duration 49.15 s

The measurement was performed in the night from February 5th to 6th 2015. A room temperature of 19.9 °C and a relative air humidity of 34.9 % were measured. There were three persons present during the measurement.

4.2.1 Global Measurement

This part of the measurement was intended to provide information about the acoustic characteristics of the entire connected space. Therefore, the impulse responses from three source positions to 10 microphone positions evenly distributed in the room were measured, which adds up to a number of 30 impulse responses. Also, the *ISO 3382* room acoustics parameters were exported in a text file for each combination of source and receiver. The positions illustrated in figure 4.4 are listed in coordinate form in table 4.1, referring to the coordinate system in figure 4.4.

The red circles around the microphone positions indicate the 1 m minimum distance to reflective surfaces as well as the 2 m minimum distance between the microphones (half a wavelength in the commonly used frequency range) according to *ISO 3382-2* [13, p. 8].

The height of the sound source and the microphones follows the assumption of standing or walking listeners, so the microphone height was set to 1.7 m. The height of the sound source was only 1.3 m for technical reasons. Figure 4.5 for example shows the first source and first

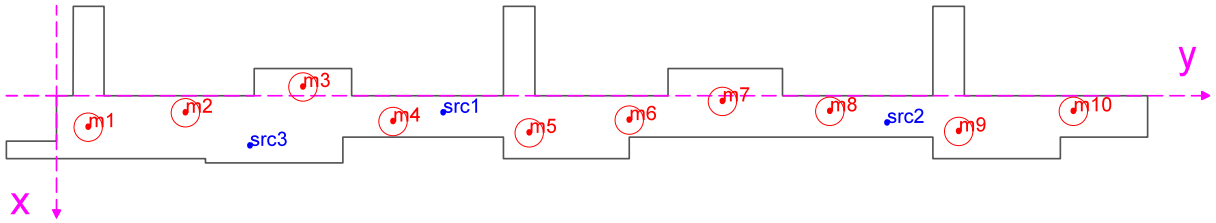

Figure 4.4: Setup for global measurement

microphone position. The speaker positions are selected in such a way that symmetric or similar configurations are avoided in order to excite preferably all relevant room modes. Furthermore, the source positions correspond to typical locations of speaking persons in everyday life and include both the working space and the hallway parts with high presence of flutter echoes. Analogous, the microphone positions cover all parts of the room, with the exception of the three exit corridors on the left side, and additionally each receives direct sound from at least two different loudspeaker positions.

Figure 4.5: Example of source and microphone positioning

4.2.2 Local Measurement

In the second part of the measurement, a part of the building 16 c where the fluttering is audible was examined in detail (see fig. 4.6). As illustrated in figure 4.7, groups of three microphone positions with different x coordinates were placed at a distance of 1 m apart in y direction, starting at $y = 21$ m (see table 4.2). The purpose of this arrangement is to examine the degree of the echo depending on the distance from the sound source at different places between the parallel walls. Each microphone triplet contained one position at a quarter of the hallway width to the first wall, one at the center of the corridor, and one placed at a third of hallway width to the opposite wall. This asymmetric positioning was chosen because of the expectation, that the sound field would be approximately symmetric to the center line and thus a symmetric

mic. id	x / m	y / m
1	2.2	2.2
2	1.2	9.0
3	-0.6	17.2
4	1.8	23.5
5	2.6	33.0
6	1.7	40.0
7	0.4	46.5
8	1.1	54.0
9	2.5	63.0
10	1.1	71.0

src. id	x / m	y / m
1	1.2	27.0
2	1.9	58.0
3	3.5	13.5

Table 4.1: Coordinates of microphone and source positions (global measurement)

arrangement presumably would not provide any additional information. The speaker was located at the center line between the walls and half a meter away from the closest microphone positions. Again, the impulse response as well as the room acoustics parameters of the path from the source to each microphone were exported. The height of the microphones and the loudspeaker were the same as with the global measurement. For time reasons, only one source position could be used. The previously mentioned 1 m radius around the microphones marking the minimum distance to reflective surfaces was not been respected, since the sound behavior caused by the presence of close walls is desired to be examined here.

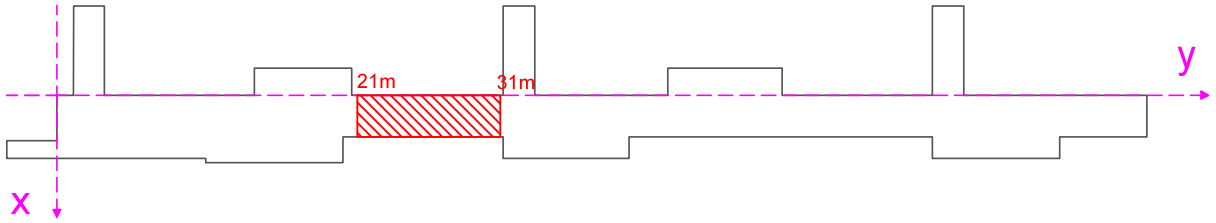

Figure 4.6: Area of detail measurement

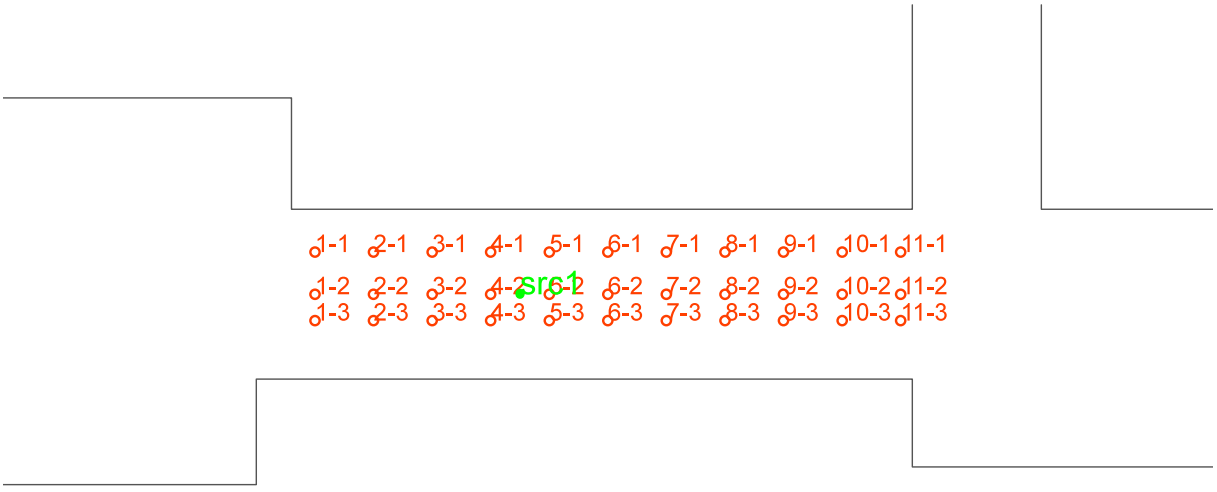

Figure 4.7: Source position and microphone positions of detail measurement

Figure 4.8: Example of measurement configuration (local measurement)

id	x / m	y / m
1-1	0.73	21
2-1	0.73	22
3-1	0.73	23
4-1	0.73	24
5-1	0.73	25
6-1	0.73	26
7-1	0.73	27
8-1	0.73	28
9-1	0.73	29
10-1	0.73	30
11-1	0.73	31

id	x / m	y / m
1-2	1.45	21
2-2	1.45	22
3-2	1.45	23
4-2	1.45	24
5-2	1.45	25
6-2	1.45	26
7-2	1.45	27
8-2	1.45	28
9-2	1.45	29
10-2	1.45	30
11-2	1.45	31

id	x / m	y / m
1-3	1.9	21
2-3	1.9	22
3-3	1.9	23
4-3	1.9	24
5-3	1.9	25
6-3	1.9	26
7-3	1.9	27
8-3	1.9	28
9-3	1.9	29
10-3	1.9	30
11-3	1.9	31

Table 4.2: Coordinates of the microphone positions (local measurement)

id	x / m	y / m
1	1.45	24.5

Table 4.3: Coordinates of the source position (local Measurement)

5 Measurement Results

In the previous section, the local conditions in the building and the measurement approach were described. In this section, the collected data will be presented and analyzed.

Since the room acoustics parameters were exported from *WinMLS* into a single text file for each transfer path from sound source to microphone, a *MATLAB* tool was written in order to provide a clear and flexible graphic representation of the measured values. In the following diagrams, the legends refer to the file names of the measured impulse responses and the text files and allow an unambiguous identification of the respective source and microphone location according to the position numbers shown in sections 4.2.1 and 4.2.2.

The names are of the form

$$\mathbf{m}x\mathbf{s}y\mathbf{p}z.* \qquad \text{example:} \quad \mathbf{m1s2p}5.txt \quad \text{or} \quad \mathbf{m2s1p}4\text{-}3.wmb\,,$$

where *m1* refers to the global and *m2* to the local measurement. The identifier s stands for the selected source and p for the microphone position. If p is followed by two numbers separated by a hyphen, the first number stands for the position in y direction and the second for the x position (see fig. 4.7). Where the name is followed by *run1* or *run2*, the measured values made a conspicuous impression and the measurement for the respective configuration was repeated. Unless specified differently, the second run, however, confirmed the first one.

5.1 Global Measurement

Figure 5.1 shows the average T_{30} curve of all source/microphone combinations of measurement 1. The mean reverberation time of all frequency bands is 1.19 s, 1.24 s if the highest and the lowest band are neglected. In both cases the average is 1.2 s if the conventional rounding to one decimal place is applied.

Taking a closer look at the collected data, the results show several conspicuities that should be considered. The T_{30} curves of each transfer path are presented in figure 5.2, showing two main peculiarities. First, there is an increase of the reverberation time below 500 Hz, and second, a noticeable parallel shift at the whole frequency range, most distinct above 1 kHz.

The transfer paths of the source/receiver combinations that show the highest peaks (at 125 Hz) are represented in figure 5.3. It naturally comes to mind, that the irregularities of microphone position 4 and 8 are caused by a flutter echo between the narrow walls, although this explanation might not be sufficient for position 9.

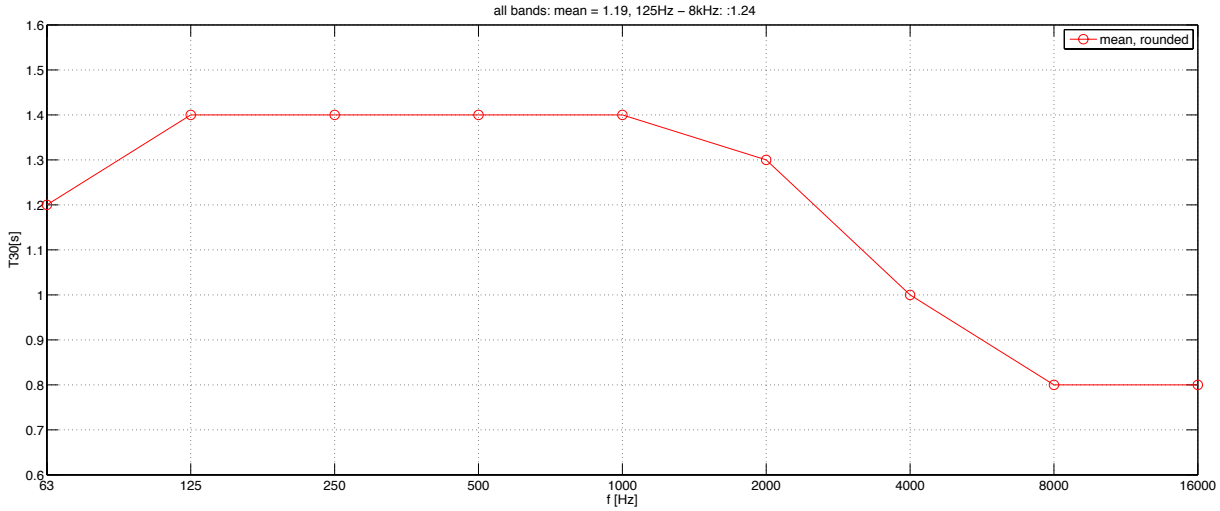

Figure 5.1: Mean T_{30} (vertical axis), rounded (global measurement). Horizontal axis: frequency in Hz

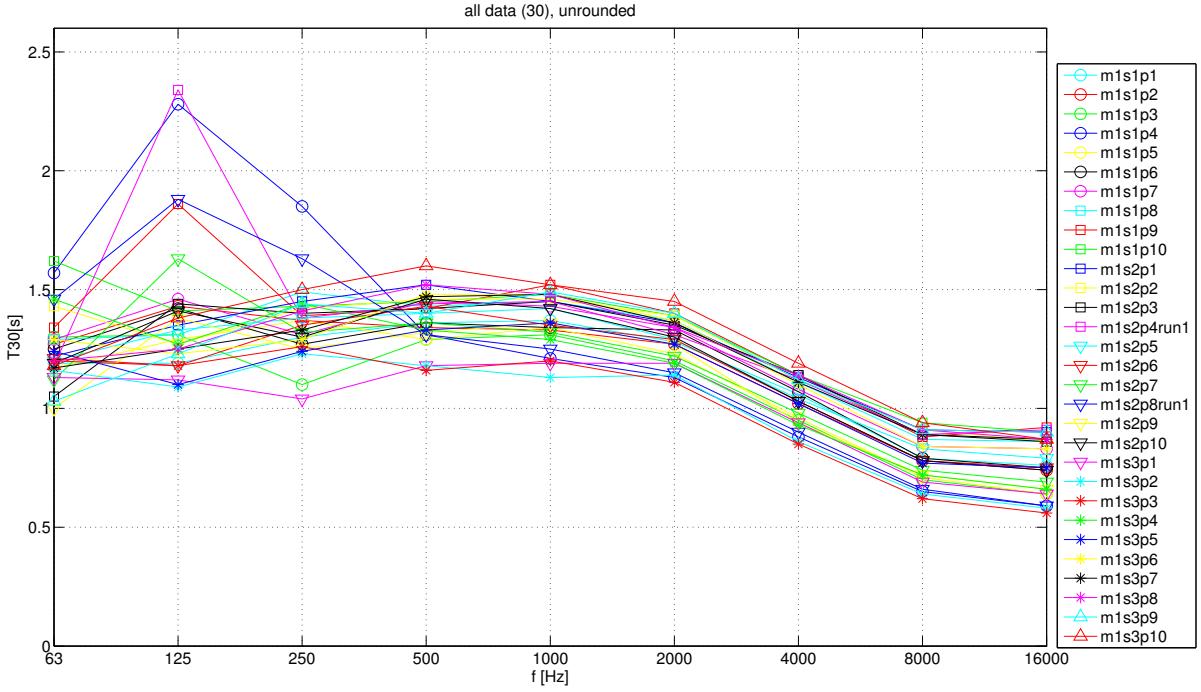

Figure 5.2: T_{30} (vertical axis), unrounded (global measurement). Horizontal axis: frequency in Hz

5.1.1 Possible Reasons for the Parallel Shift

The parallel shift observed in the T_{30} measurement is closely connected to the distance between the microphone and the sound source. In order to verify this, for each source, in figures 5.4 to 5.6, the reverberation times are plotted band-wise from 125 Hz to 16 kHz as a function of the distance of each microphone position to the respective source. The source position is indicated by a red

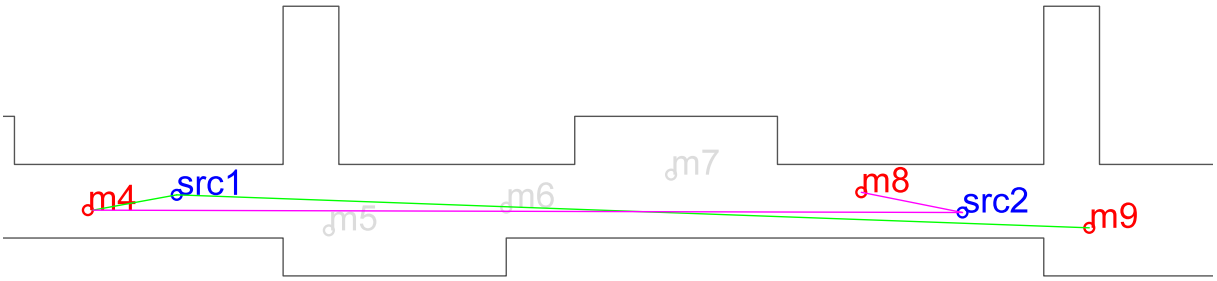

Figure 5.3: Transmission paths that produce a peak at 250 Hz

arrow and the dots on the curves mark the microphone positions 1 to 10 (from left to right). Indeed a trend is observable: For each loudspeaker position, the reverberation times tend to increase with growing distance. At low frequencies (below 250 Hz), major deviations from the trend can be observed.

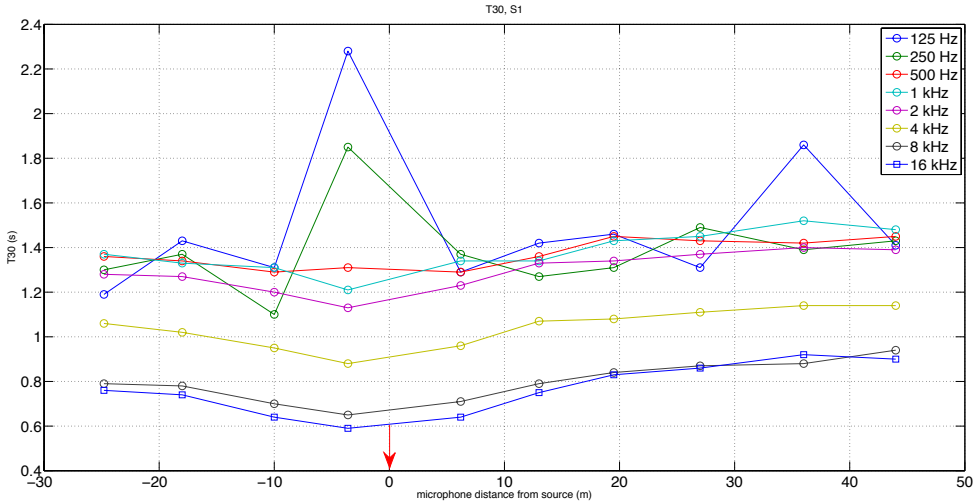

Figure 5.4: Reverberation times in regard to the microphone position (source 1). Vertical axis: T_{30} in s, horizontal axis: distance between microphone and sound source in m

In a reverberation time measurement performed at St. Stephen's Cathedral, Vienna, a similar effect was observed. The problem was discussed in a project work by P. Gutmann [20] and it was examined, whether the reason for the parallel shift lies in the way energy propagation takes place in large enclosures. If, for example, a large room is excited by impulsive sound at the front end, the sound energy in this part of the room will increase rapidly and spread out in space. When the sound waves reach the boundaries of the enclosure, absorption and reflection take place. Thus, the sound energy close to the source decreases due to absorption and propagation in the room. When the energy equilibration process is completed, only the contribution of absorption remains. In the rear part of the room, initially, energy from the front end constantly arrives and slows down the decay process (caused only by absorption loss), until a stationary energy distribution is accomplished [20, p. 102 ff.]. Hence, the decay in the rear part takes place slowlier at the beginning, and longer reverberation times will be measured with increasing distance between source and receiver.

Another possible reason given for the parallel shift was the long attack time (level increase) at great distances that could lead to evaluation errors if the beginning of the decay curve can not be determined clearly [20, p. 50 f.].

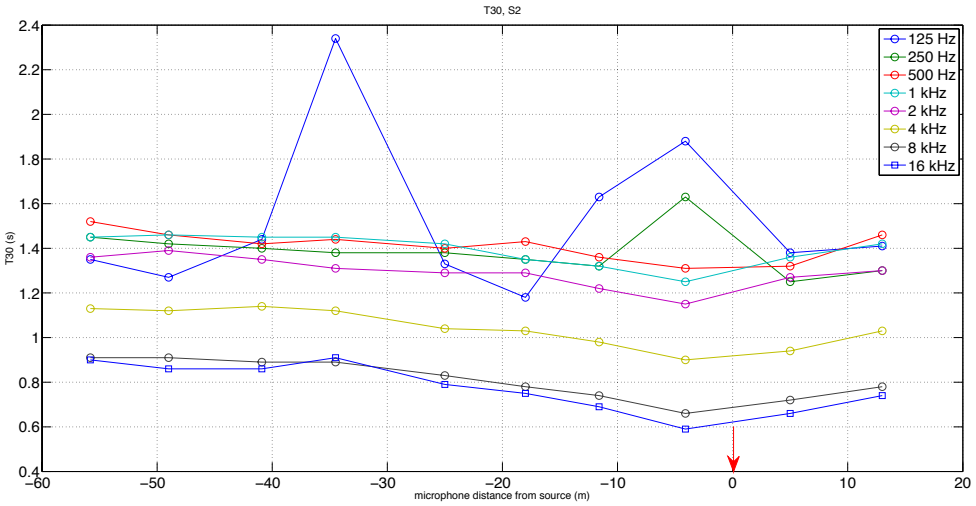

Figure 5.5: Reverberation times in regard to the microphone position (source 2). Vertical axis: T_{30} in s, horizontal axis: distance between microphone and sound source in m

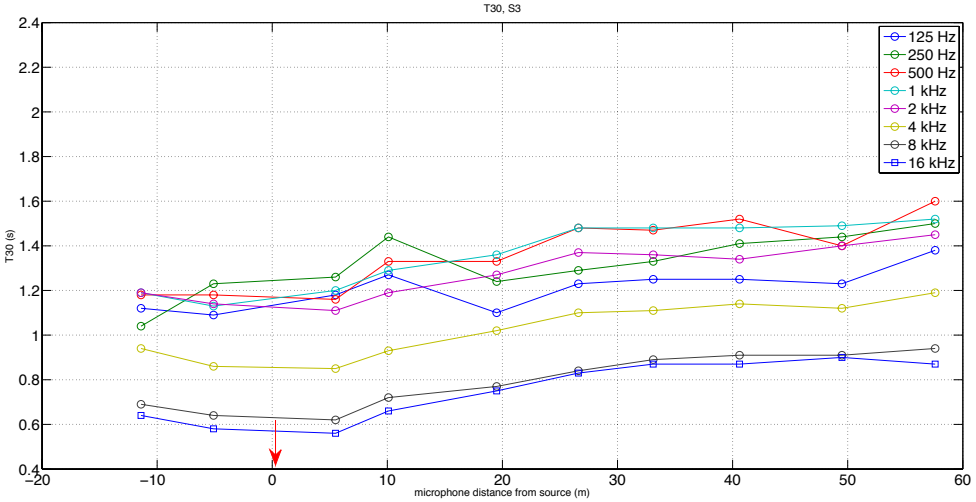

Figure 5.6: Reverberation times in regard to the microphone position (source 3). Vertical axis: T_{30} in s, horizontal axis: distance between microphone and sound source in m

However, for source 3 in figure 5.6, the low frequency curves are rather inconspicuous. This might be caused by the possibility that source 3 did not excite the resonances, which could have led to the deviations described above, as this source is the only one located at a relatively wide part of the hallway.

5.1.2 Possible Reasons for Outliers

Gutmann showed in [20], that there is a connection between the spatial distribution of the nodes and antinodes of a stationary wave and the spatial distribution of the measured reverberation time in such a way that longer reverberation times are measured at the antinodes. This could be a reason for some of the outliers, especially as one can expect strong resonances between the concrete walls. If a standing wave builds up, the nodes, where no oscillation takes place, and the antinodes, which are the points where the sound pressure reaches its minimum and maximum values, are stationary. Because the energy has its maximum at the antinodes, a reverberation time measurement at these locations would result in a rather short value, since, when the source is turned off, the standing wave collapses, causing a quick energy decay. In contrast, at the

nodes, the minimum energy level was already reached, and initially, after turning off the source, the level actually increases before dropping again, which could result in measuring a rather long reverberation time [20, p. 55 f.]. The experiments performed in [20] support this hypothesis.

Since the T_{30} values theoretically should be the same as the T_{20} values, it could be helpful to graphically represent the difference between the two parameters in order to find evaluation errors, like done in figure 5.7. The figure shows, that the difference gets bigger at low frequencies, which indicates a growing evaluation uncertainty if frequency decreases. Noticeable is the great deviation of one of the curves. It has been noticed during measurement and thus, the measurement was repeated. Indeed, using the second data set, the deviation between the reverberation times is much lower and the standard deviation is below 0.1 s. The T_{30} measurement is only

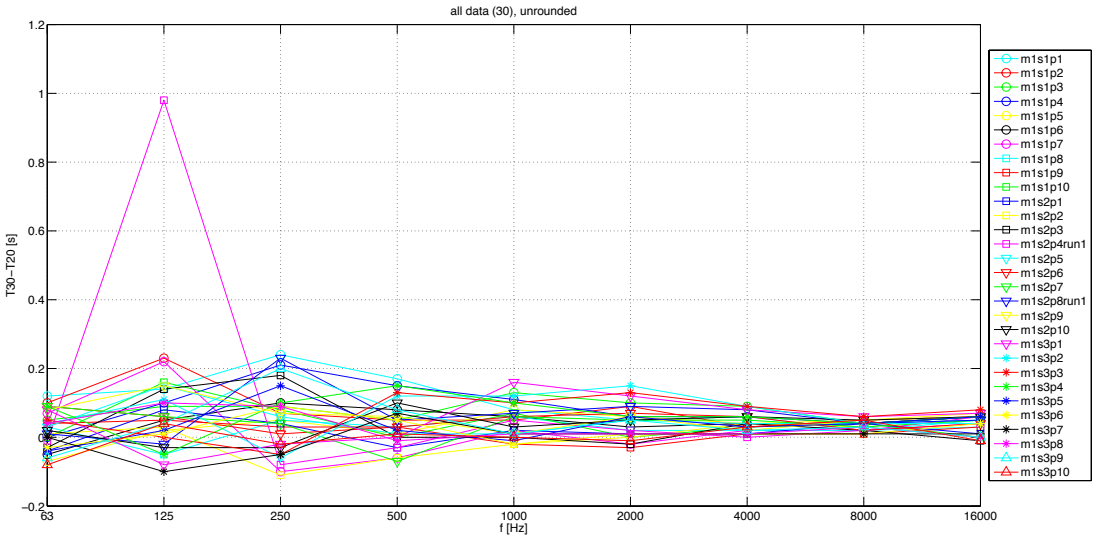

(a) all curves

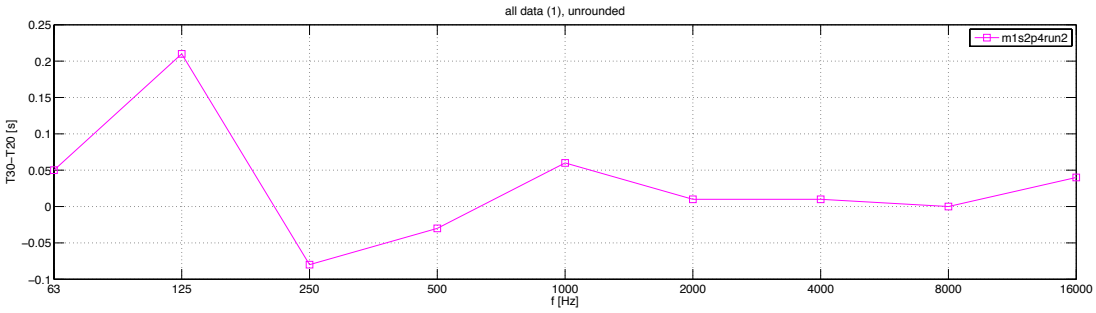

(b) source 2, position 4, run 2

Figure 5.7: Difference between T_{30} and T_{20}. Vertical axis: $T_{30} - T_{20}$ in s, horizontal axis: frequency in Hz

valid if the receiver is far enough away from the sound source. A helpful measure is the quotient of reverberation time and early decay time, which has been introduced in [20]. Because in the near field of the loudspeaker, after turning it off, there is no direct sound anymore and the sound level will decay quickly, the early decay time will be shorter than the T_{30} and the quotient is greater than one. At a larger distance, the reverberation time will be equal to or smaller than the early decay time and so T_{30}/EDT will be equal to or smaller than one [20, p. 57 ff.]. Of course, this is only a rough indication, the specific demarcation is difficult.

A comparison of the parameter T_{30}/EDT between the global and the local measurement could provide information whether individual measurement points were located in the direct sound field of the respective source, since most of the microphones in measurement 2 are located close to the loudspeaker. The boxplot charts in figure 5.8 show far higher outliers for the local

measurement (note the different scaling of the y-axis). Also, no connection was found between the high T_{30} values and the T_{30}/EDT curves. Therefore, it is assumed that the outliers are not caused by a too small distance between receiver and source.

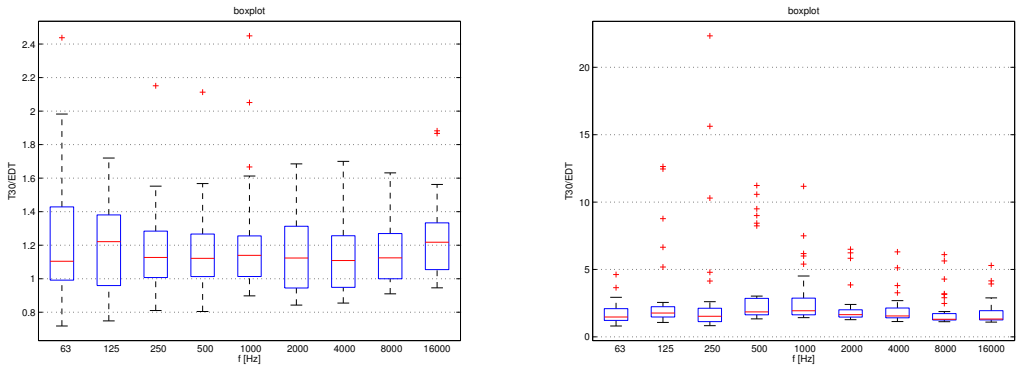

(a) global measurement (b) local measurement

Figure 5.8: Comparison of T_{30}/EDT (vertical axis). Horizontal axis: frequency in Hz

5.1.3 Reverberation Time in Accordance With ISO 3382-2

The validation of the T_{30} measurement requires to consider the available signal-to-noise ratio. Figure 5.9(a) shows a box plot of the SNR of the impulse responses. The lowest levels are reached at the 63 Hz and 16 kHz band. The effective decay range in figure 5.9(b), which is a parameter delivered by *WinMLS* that provides information about the available SNR in the decay curve, is above the 35 dB needed for T_{30} evaluation, except for the highest and lowest band, which therefore should be excluded from the calculation of the reverberation time in accordance to *ISO 3382-2*. This means that the T_{30} measurement is expected to be valid between 125 Hz and 16 kHz.

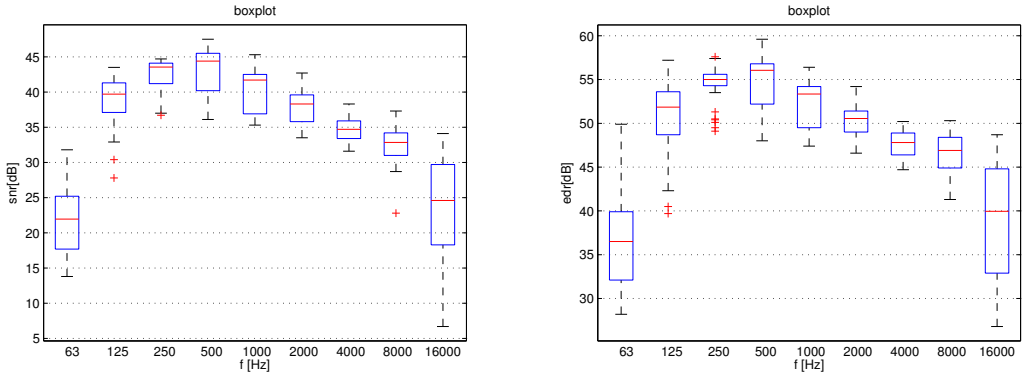

(a) Signal-to-noise ratio (b) Effective decay range

Figure 5.9: Signal-to-noise ratio and effective decay range (vertical axis). Horizontal axis: frequency in Hz

In order to determine the reverberation time defined in *ISO 3382-2* [13], a few more things must taken into consideration. Because the reverberation time is only defined in diffuse sound field,

a minimum distance d_{min} between source and receiver must be maintained:

$$d_{min} = 2\sqrt{\frac{V}{c\hat{T}}} \tag{5.1}$$

The resulting minimum distance is about 6 m if the Volume V is 3750 m^3, the sound velocity c is 343 $\frac{m}{s}$, and the required estimate value of the reverberation time $\hat{T}$ is set to the already calculated mean value of 1.2 s.

In figure 5.10, the minimum distance is illustrated by green circles around the source locations. As a result of this requirement, the number of available independent source/receiver combinations decreases from 30 to 24, because, for each source position, the two receiver positions closest to the speaker location cannot be used. Nevertheless, a more than sufficient number of independent source/receiver combinations remains, since, according to the standard, the required number for a precision measurement is at least 12. The standard requires a frequency range

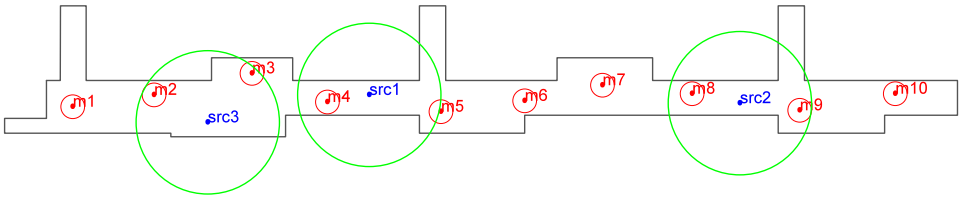

Figure 5.10: Minimum distance around sound sources

of at least 125 Hz to 4 kHz, which is respected here, since the SNR is sufficient from 125 Hz to 8 kHz. The reverberation time is calculated by averaging of the mean reverberation times of each source position, including the microphone locations outside the 6 m radius (see table 5.1). Illustration 5.11 shows the result. The mean reverberation time is 1.3 s.

		T_{30} in s						
src. ID	mic. IDs	125 Hz	250 Hz	500 Hz	1 kHz	2 kHz	4 kHz	8 kHz
1	1,2,3,6,7,8,9,10	1.4	1.3	1.4	1.4	1.3	1.1	0.8
2	1,2,3,4,5,6,7,10	1.5	1.4	1.4	1.4	1.3	1.0	0.8
3	1,4,5,6,7,8,9,10	1.5	1.4	1.4	1.4	1.3	1.1	0.8
average		1.5	1.4	1.4	1.4	1.3	1.1	0.8

Table 5.1: Reverberation time in accordance to ISO 3382-2*: Values used for calculation (rows 3 to 5) and spatial average for the whole building (row 6).*

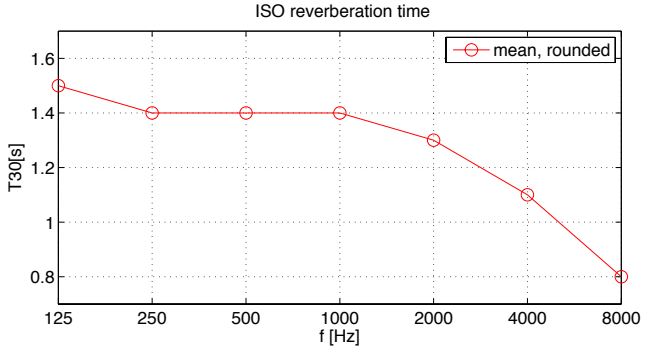

Figure 5.11: Reverberation time in accordance with ISO 3382-2

5.2 Local Measurement

The goal of the second, local measurement was to examine the sound field behavior at a certain area in detail. Nevertheless, it makes sense to compare the reverberation times of the local measurement with those of the global measurement. In figure 5.12, you can see the unrounded average reverberation times of measurement 1 and 2. It is eye-catching that the values of

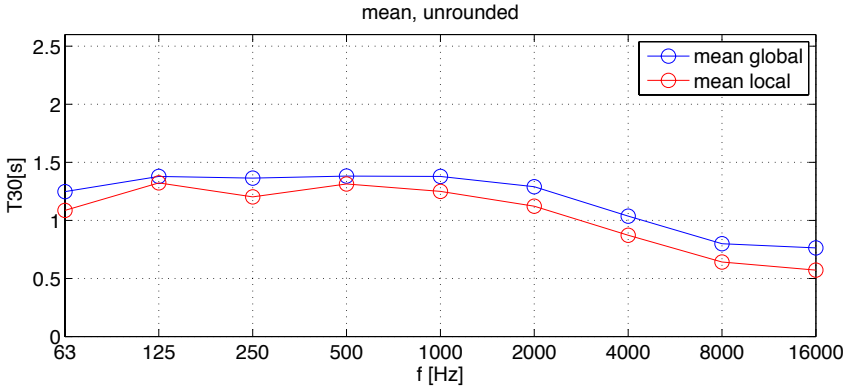

Figure 5.12: Unrounded T_{30} curves of measurement 1 and 2

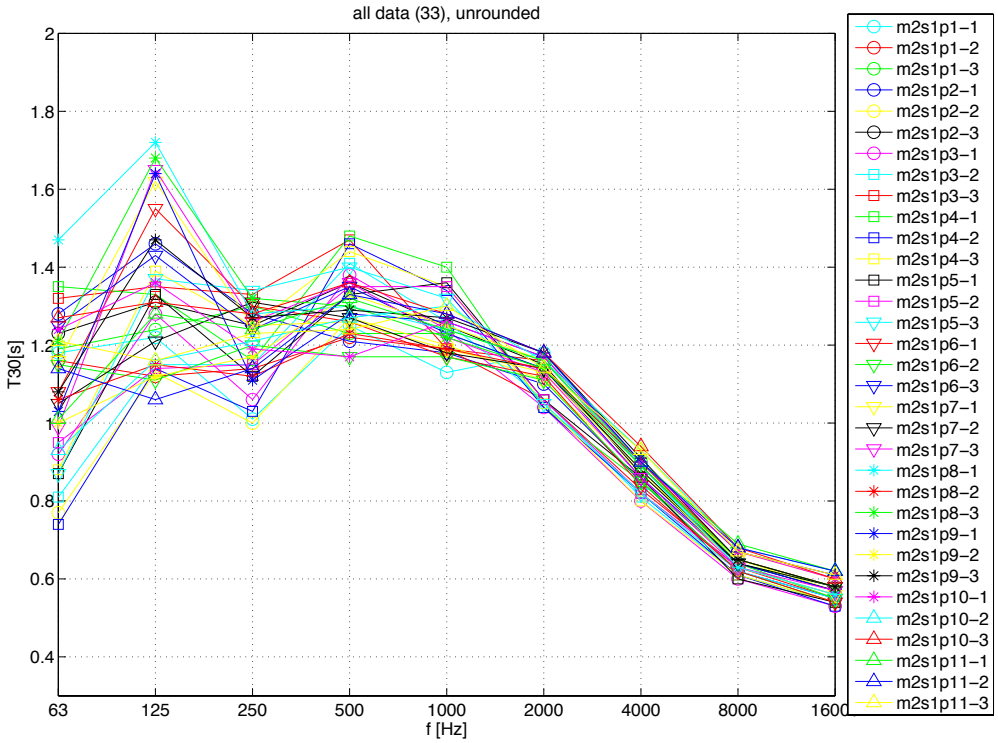

Figure 5.13: All T_{30} curves of measurement 2

the local measurement are lower for all frequencies, and in the higher range, there is an almost constant offset between the curves. This might be caused by the already examined distance dependency of the measured reverberation time, since the maximum distance between source and receiver in this measurement is comparable to the minimum source/receiver distance in the global measurement; it can also be assumed, that most of the microphone positions are located

inside the direct sound field radius. Moreover, the parallel shift noticed in section 5.1.3 is also observable in the detail measurement, which can be seen in figure 5.13. It can be shown that, for high frequencies, the measured T_{30} values increase with distance to the source. The distribution of the reverberation times is much wider at low frequencies. For example, the standard deviation at 125 Hz (0.2 s) is almost 8 times higher than the one at 8 kHz, what is presumably caused by room modes respectively the appearance of flutter echoes in the low frequency range.

5.2.1 Room Resonances and Flutter Echoes

For examination of the strength of room modes depending on the distance to the source, the impulse responses already used for T_{30} calculation have been transformed into the frequency domain. Figures 5.14 to 5.16 show the power spectra at each microphone position for the subindices 1 to 3 (compare fig. 4.7). The frequency is plotted on the horizontal axis and the vertical axis shows the microphone position from 1 to 11; the loudspeaker was positioned between 4 and 5. Several dark red stripes at constant frequencies are noticeable in the plots. They indicate the frequencies, where resonances occur. Only room modes in x direction will appear in the plots, as the resonances in y direction occur at very low frequencies and, therefore, are not relevant. The lowest resonance frequency between the walls of the corridor in x direction, which was not visible in the spectra, would be at 59 Hz. For calculation of the room mode frequencies, see equation 2.3 on page 11. The second mode at about 118 Hz, however, is visible in figures 5.15 and 5.16. Strong resonances at all sub-positions can be observed at about 237 Hz, which is the fourth mode. Even at 355 Hz and 473 Hz (sixth and eighth order, see figure 5.16), slight resonances appear.

The illustrations clearly show that the level of the resonances decreases with growing distance from the source. In some plots, certain frequencies do not appear, which can be explained by the different x positions of the receivers of each plot: For instance, the microphones with subindex 1 (figure 5.14) were located at a quarter of the hallway width. At this point, the second room mode at 118 Hz has a pressure node and therefore no oscillation can be found with pressure transducers like the omnidirectional microphone capsules used in the measurement.

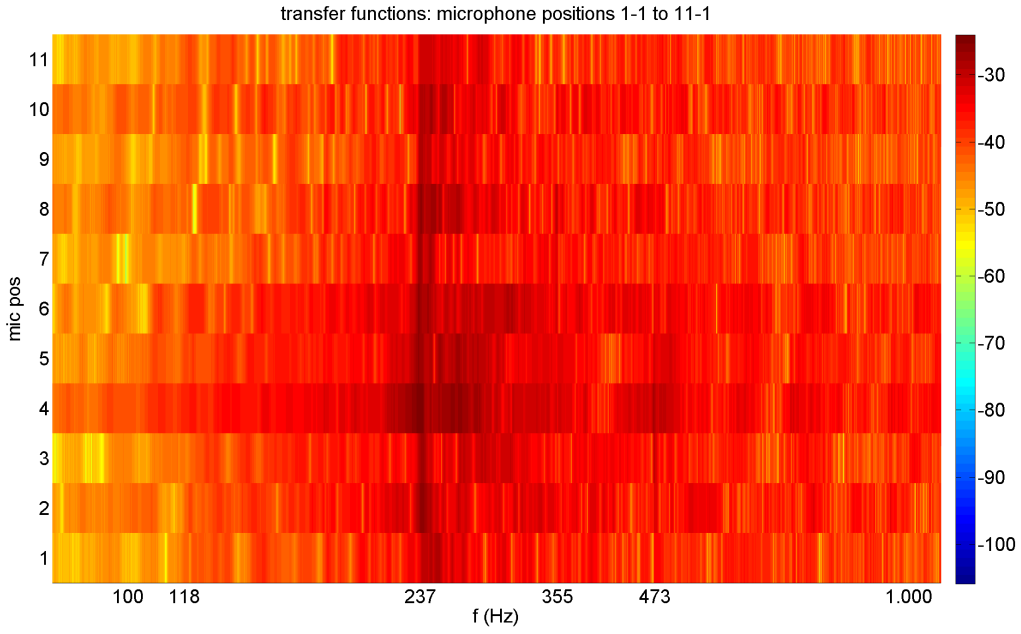

Figure 5.14: FFT of microphone positions 1 to 11, sub-position 1

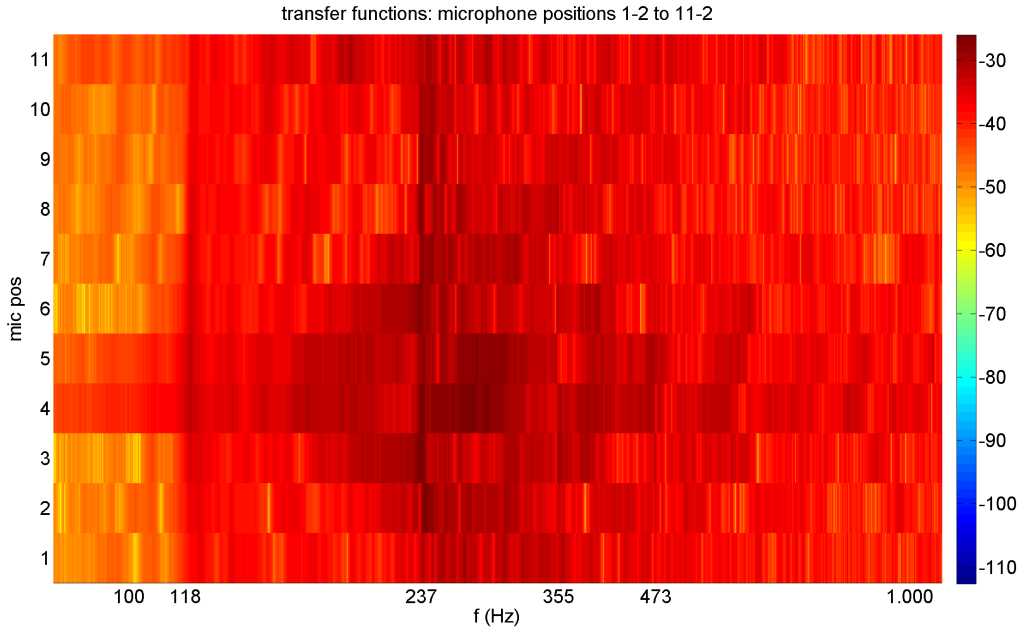

Figure 5.15: FFT of microphone positions 1 to 11, sub-position 2

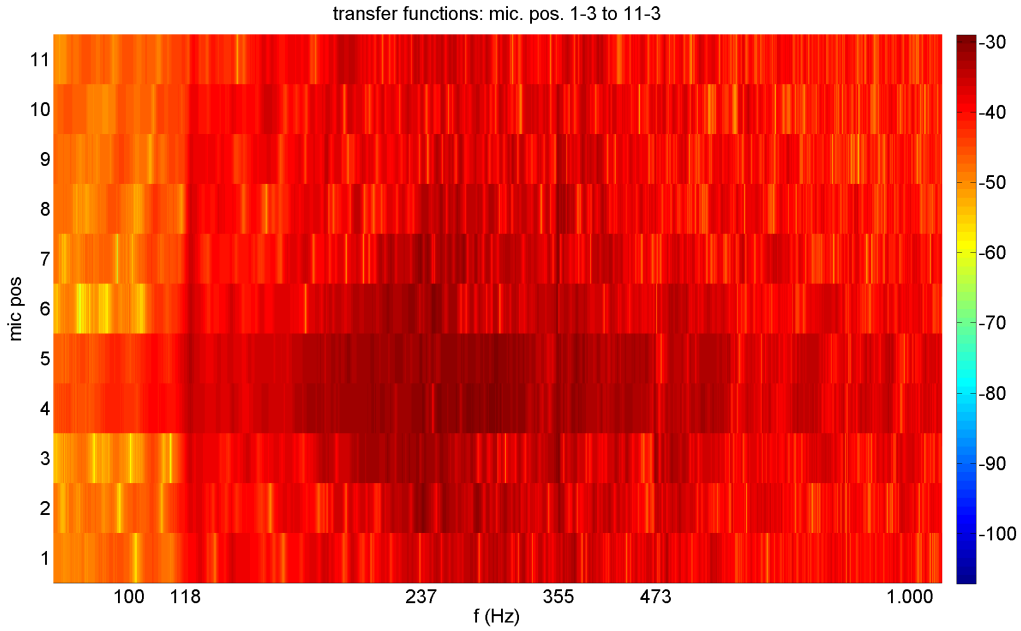

Figure 5.16: FFT of microphone positions 1 to 11, sub-position 3

The plots 5.14 to 5.16 show the strong room modes that occur at the narrow parts of the hall in the frequency domain.

Flutter echoes can be looked at as a series of room resonances excited by impulsive sound [21, p. 217]. Showing the temporal character of the phenomenon - the flutter - nevertheless is more difficult. In the impulse responses of the local measurement, recorded close to the loudspeaker, flutter echoes are clearly audible. Increasing the distance from the source, the flutter gets less present but does not disappear.

Various approaches on the detection of echoes are presented in section 5.4.

5.3 Reverberation Time and Intelligibility

ÖNORM B 8115-3 specifies reference values for the reverberation time in rooms with regard to the desired type of usage. The following empirical formula calculates the optimal reverberation time T_{opt} for speech usage depending on the volume of the enclosure [22, p. 5].

$$T_{opt} = \big(0.37\,\lg\Big(\frac{V}{\mathrm{m}^3}\Big) - 0.14\big)\mathrm{s} = \big(0.37\,\lg\big(3750\big) - 0.14\big)\mathrm{s} \approx 1.2\,\mathrm{s} \tag{5.2}$$

The ratio of measured and recommended reverberation time $\frac{T}{T_{opt}}$ is shown in illustration 5.17 (black). It should not exceed the upper/lower limits indicated by the red lines, whereby its target value, of course, is 1.

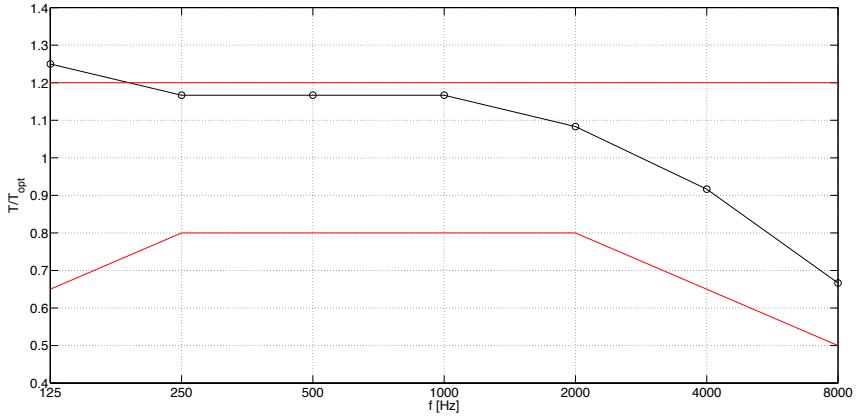

Figure 5.17: Black: $\frac{T}{T_{opt}}$ (vertical axis), red: upper and lower limits according to ÖNORM B 8115-3 *p. 6 (read off). Horizontal axis: frequency in Hz*

This requirement is fulfilled for all frequency bands but 125 Hz. However, there exist some arguments for questioning the relevance of this consideration.

By reason of the shape of the building, the reverberation time values show strong local variations. Probably a mean T_{30} for the whole building is of limited significance.

It might be difficult to say how to define the volume, because the enclosure probably can be imagined as a structure consisting of a number of coupled rooms that have to be looked at separately. These could be different longitudinal parts, the exit corridors and parts of the upper stories. Splitting up the room into smaller volumes would lower the reference value T_{opt} and presumably lead to additional violations of the upper limit of $\frac{T}{T_{opt}}$ in the sub-parts.

Furthermore, the application of this speech criterium might not be suitable for this type of building, because the formula above is certainly more reliable if applied on rather simple-shaped rooms (cuboid etc.).

Only looking at the T_{30} values might also not be of great use. The disturbances are maybe not mainly caused by a too long reverberation time but the character of the decay, which is colored by flutter echoes and room modes. It might therefore be less the case of technical intelligibility problems but of a subjectively unpleasant sound character of the reverberation.

The criterium D_{50} is used to objectively review speech intelligibility. It is the ratio of the energy arriving in the first 50 ms to the total energy. For good intelligibility, it should be greater

than 50 %. Figure 5.18 shows the statistical evaluation of the D_{50} values of measurement 1, containing all measured impulse responses. Very good as well as poor values can be observed. Having a closer look on the values for the single impulse responses, it can be seen that low values mainly occur at remote positions, the values close to the source are better, of course. Since the hall is not an auditorium or a class room, perfect intelligibility over more than 10 m can not be a requirement.

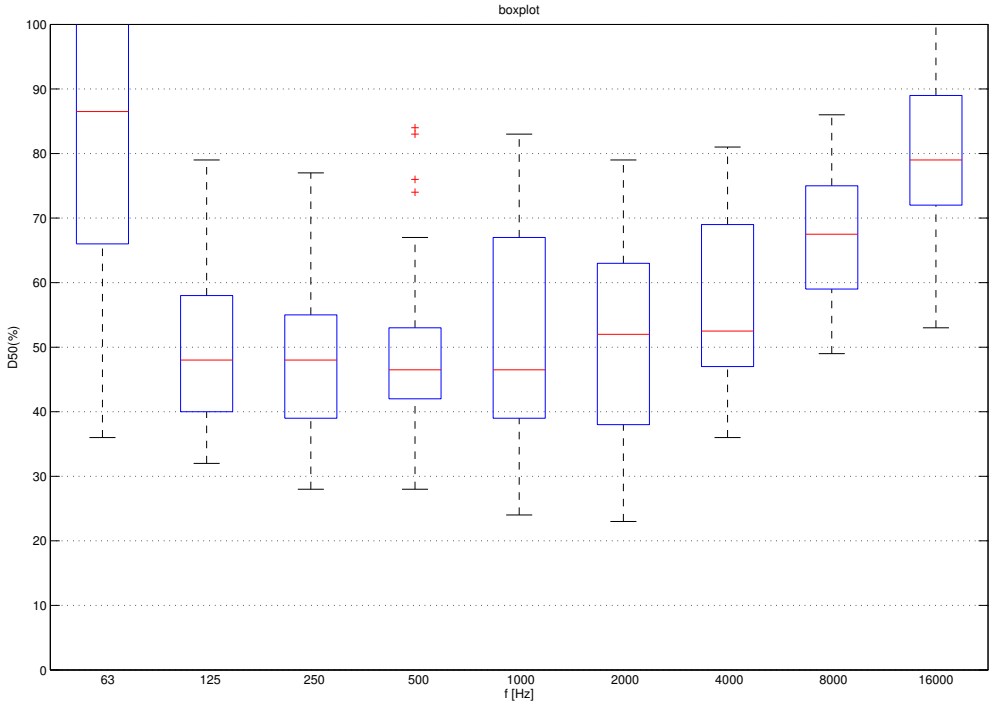

Figure 5.18: Statistical evaluation of the D_{50} values of measurement 1

5.4 Detection of Flutter Echoes

Short Literature Research

The automatic detection of echoes in impulse responses can be of great use. Common applications for echo detection are for instance in radar technologies and telecommunications. In acoustics, the detection of echoes and the evaluation of a psychoacoustic measure for the echo disturbance can be used for an objective comparison of measurements in different rooms. Moreover, an automatic detection can be part of a simulation software, providing information about the risk of echoes in a room model without requiring the software operator to evaluate the calculated impulse responses by hearing. In the following, an overview of different approaches to this topic is presented.

In 1965, H. Kuttruff introduced a property that he called *temporal diffusion*. It compares the absolute maximum of the autocorrelation to the next highest maximum [23]. It is used to show the amount of irregularity in the reflections of the impulse response; a random distribution is desired, since it does not lead to coloration like flutter echoes do.

K. Środecki made further investigations on the temporal diffusion and sound coloration in 1994 and also proposed the use of cepstral analysis for this purpose [24].

A different approach was made by Dietsch in 1983 [25], based on the *center time* t_S, which is a measure for the room impression and intelligibility [1, p. 197]. The echo criterion (EK) was defined as the difference quotient

$$EK(\tau) = \frac{\Delta t_S(\tau)}{\Delta \tau_E} \,, \tag{5.3}$$

where t_S is determined as follows:

$$t_S(\tau) = \frac{\int_0^\tau t \cdot |p(t)|^n \mathrm{dt}}{\int_0^\tau |p(t)|^n \mathrm{dt}} \,. \tag{5.4}$$

The constants n and τ_E are empirically determined for certain echo thresholds and requirements on the room [26, p. 3 ff.].

J. Abel and P. Huang assumed a gaussian distribution of the coloration-free diffuse reverberation and developed a property that "counts samples lying outside a standard deviation in a given impulse response window and normalizes by that expected for Gaussian noise" [27, p. 1].

Due to the repetitive character of flutter echoes, they are often perceived as a coloration. This is why echo criteria that perform well with single echos might experience difficulties recognizing flutter echoes. One might therefore consider using methods that operate only the frequency domain like Salomons' *A0 criterion* that analyzes the modulation depth of the spectrum [28, p. 13].

Applying the Autocorrelation on Measured Impulse Responses

In practice, the metrological detection of the flutter echoes, which, until now, have been treated mostly on a subjective level, turned out more difficult than expected. Due to the large number and density of reflections, it is difficult to directly identify single echoes in the impulse responses.

But since the flutter echo ideally consists of periodically repeated pulses, it maybe can be found in an impulse response by applying signal processing methods like the autocorrelation function, an operation that is able to reveal hidden signal periodicities.

The application of Kuttruff's temporal diffusion, however, did not yield any significant results in this measurement.

But looking at the autocorrelation plots of the measured impulse responses could provide additional information. For a detailed analysis, the impulse responses have been filtered by an octave filter bank before. Figure 5.19 shows the absolute value of the autocorrelations of the two microphone positions 4 (left) and 8 (right) of the global measurement. Flutter echoes were only audible at these positions, if the sound source was located in the same part of the room and thus excited the flutter. In the upper diagrams, the source was near microphone 4 (source 1), and the lower diagrams show the results if the loudspeaker was near microphone 8 (source 2). One can see the change in the 125 Hz band very clearly if flutter echoes occur.

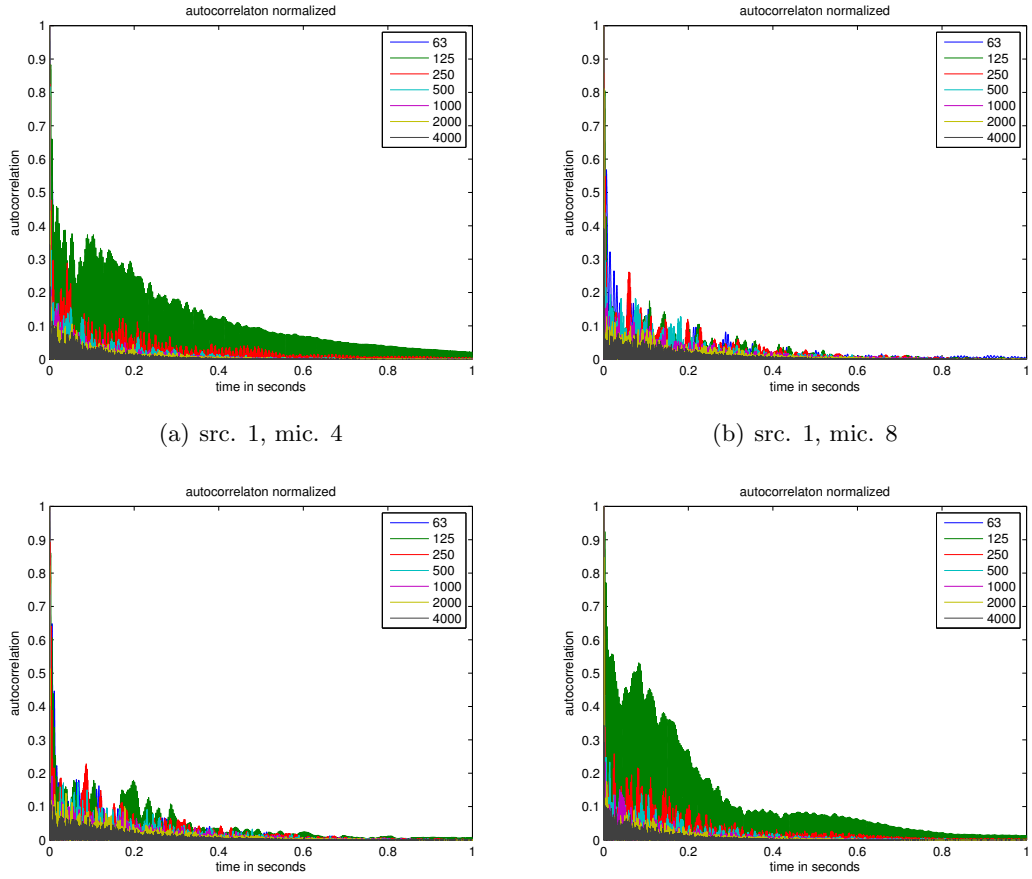

(a) src. 1, mic. 4

(b) src. 1, mic. 8

(c) src. 2, mic. 4

(d) src. 2, mic. 8

Figure 5.19: Right-sided autocorrelation of octave-band filtered impulse responses of measurement 1. Sound source and receiver where in the same area in (a) *and in* (b)

6 Simulation

In this chapter, various strategies for avoiding flutter echoes are presented. After a comparison of a model in *CATT-Acoustic* of the building Inffeldgasse 16 c and the measurement, countermeasures are reviewed by means of simulations, using both rectangular room models and a model of the actual building.

6.1 Comparison Between Simulation and Measurement

In order to be able to review optimization measures in a simulation, a model in *CATT-Acoustic* was created. The full-complexity model is shown in figure 6.1. It is based on the construction plans of Inffeldgasse 16 c.
After completing the model, the first step was to find out if the simulation yields results which are similar to the measurement data.

The first runs showed high deviations between measurement and simulation, although the absorption and scattering values of the extensively used material of concrete are known, since it is a very common construction material.

Figure 6.2 shows the average of the computed T_{30} values of some of the source/receiver combinations (thick blue/red lines) that were also used in the global measurement, compared to the mean reverberation time (dotted gray line). The thick blue line corresponds to the measures calculated from the impulse response, while the red one is computed by sound energy ray tracing. To shorten the calculation process, only source 1 and 2 and half of the microphone positions were used (those with even ID numbers). At lower frequencies, the calculated values differ by 0.5 s in upward direction from the measured values. The tendency is the same in the reproduction of the local measurement (all microphone positions on the center axis of the hallway were used), which is shown in figure 6.3. It is interesting that, in contrast to the first simulation, there appears to be a large difference between the impulse response and the energy values at low frequencies. This maybe indicates a low significance of the simulation in this configuration.

It can not be assumed, that the difference at low frequencies is caused by the additional materials on the walls neglected in the simulation, which are primary posters (normal paper). The deviations might rather be caused by the high complexity of the model and the special geometry, also leading to a large dependency of the measured T_{30} on the source and receiver positions. A lot more sources and receivers as well as many more sound rays than usual would be required for a reliable simulation, which unfortunately could hardly be done for time reasons since the duration of computation is in the order of days. In addition, the estimated reverberation time values vary a lot if the scattering coefficients of the surfaces are slightly changed.

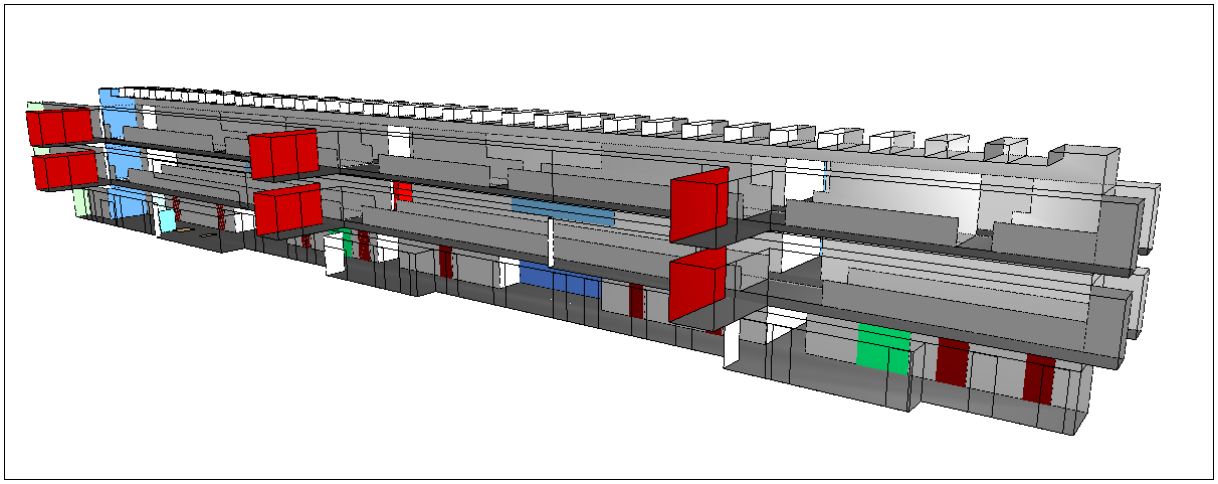

(a) external view

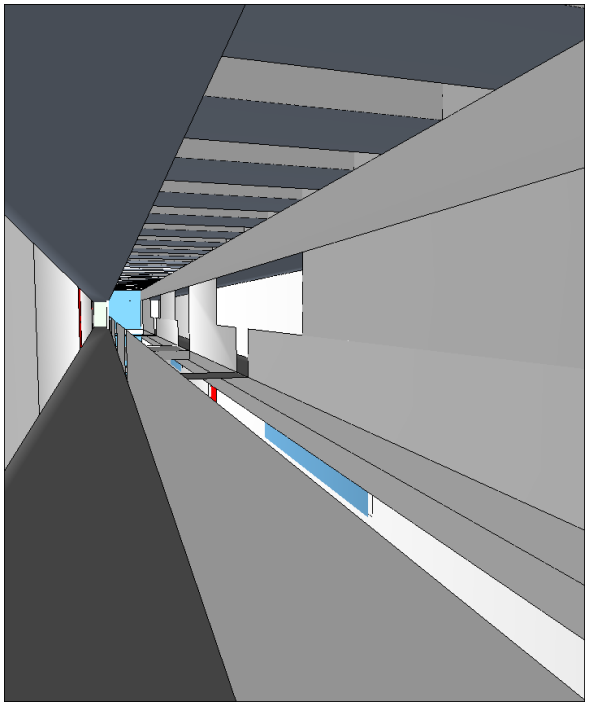

(b) inside view 1

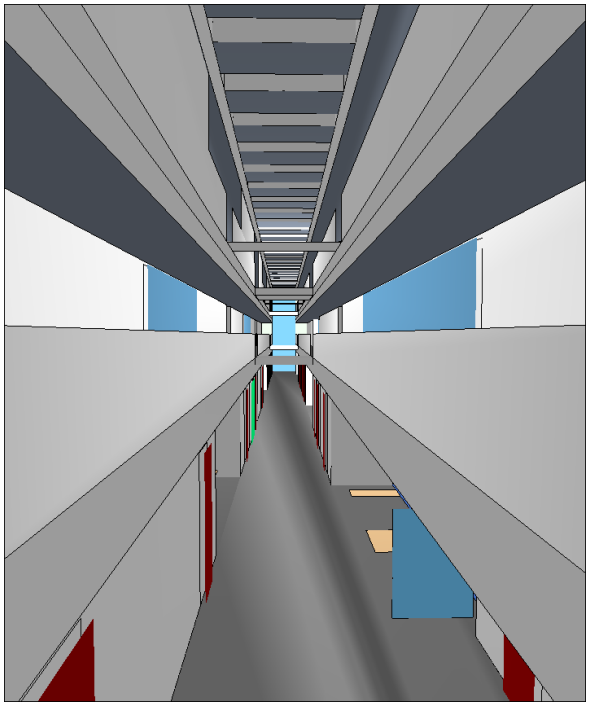

(c) inside view 2

Figure 6.1: Model of building 16 c in CATT-Acoustic

The thin blue and red lines in figure 6.2 show the calculated reverberation time values according to the formulas of Sabine and Eyring. Both the measured and the simulated data are significantly higher. This shows, that the empiric reverberation time formulas are not applicable to any arbitrary room. Presumably, the difference occurs because the assumption of diffuse sound field conditions is invalid here.

Trying to calibrate the model based on the measurement results, it turned out to be a difficult task to find suitable absorption values for some surfaces. For example, the absorption coefficients of the perforated metal ceiling covering, which is the most effective absorber in the building by far, had to be modified by trial and error and had a large influence on the calculated reverberation times. Moreover, to get closer to the expected results, some unrealistic absorption

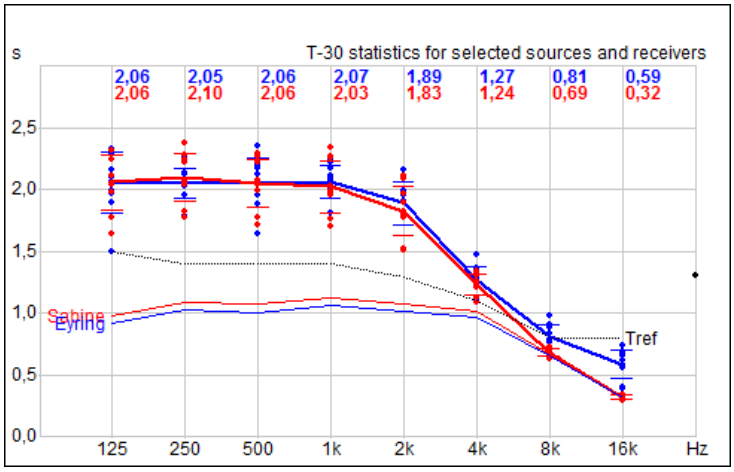

Figure 6.2: Simulation, measurement 1: T_{30}

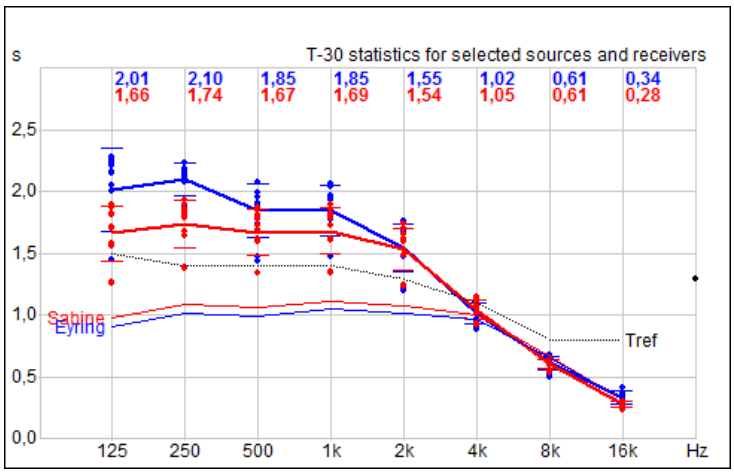

Figure 6.3: Simulation, measurement 2: T_{30}

values of the walls - the absorption coefficients of concrete are well-known - were needed.

These adjustments were made using the reverberation time estimation function of *CATT-Acoustic*. The calculated results in a detailed simulation differed from the estimation, probably caused by a too low number of sources/receivers and the scattering settings, making a calibration almost impossible.

Another problem could be that maybe T_{30} is not the best way to evaluate rooms with high complexity, since the decay curves can be deformed by coupled room effects and the occurence of echoes.

The results suggest that it might be best to only use the model of 16 c for the purpose of qualitative examinations, for instance the dependency of the visible flutter echo in the impulse responses on countermeasures. Also, maybe a simplified model with less detail in planes which are remote from the place of measurement (e.g. the upper stories) might be beneficial, because the calculation process is shortened and it is possible to use more sound rays without extending the duration of computation.

6.2 Preventing Flutter Echoes

At this point, several measures will be presented that can be applied in rooms where flutter echoes occur. Some of the strategies are preventive measures and should be taken into consid-

eration during the architectural design process, whereas others can be used in rooms already built. The strategies can be divided into three basic types that will be described in the following.

6.2.1 Application of Absorbers

The first countermeasure one can think of is to reduce the amount of reflected sound between the walls that generate the flutter. This can be done by the use of absorbent building materials or by applying sound absorbers on the walls. For this purpose, various different ways exist offering creative possibilities in design, which are not discussed here.

Instead, let us have a look on the case of having little design freedom. If the characteristic architectural features of a building must not be changed, like for instance in historical buildings or other spaces of architectural value, very decent measures are required.

One quite new possibility could be the use of transparent micro-perforated foils that are mounted at a certain distance to the walls, in front of windows or as sails anywhere in the room (for example, see illustration 6.4).

(a) (b)

Figure 6.4: Example of transparent foil absorbers. Barrisol - Normalu SAS. [Online], viewed: 7 May 2015, available: http://microsorber.net/service/bildergalerie

In order to see the effect of micro-perforated foils on flutter echoes, a model of a rectangular room with dimensions similar to the part of building 16 c, in which the local measurement took place, was created. The large opposite walls, which generate the flutter echo, and the floor between them were modeled with the acoustical properties of concrete with very low absorption and scattering. The three walls left had a comparatively high overall absorption (arbitrary / adjusted by ear), so that the flutter echo appeared clearly in the impulse responses. Also high scattering coefficients were used in order to make the simulation comparable to longer and higher rooms (like 16 c), where a large number of diffuse reflections arrives from remote walls.

In this simulation, perforated foils were applied at distances of 30 mm, 50 mm and 100 mm to the reflective walls. The absorption coefficients are shown in figure 6.6.

One sound source and three receivers at the center axis of the room were used. The constellation was the same as in the local measurement (microphone positions 6, 8 and 11). The only difference was that in the simulation source and receivers are in the same height (1.5 m), because the flutter echoes are expected to be stronger if receivers and source are in a common plane orthogonal to the walls.

The resulting impulse responses of two of the microphone positions are shown in figure 6.7 (blue/foreground) compared to the impulse response without absorbers (green/background). It

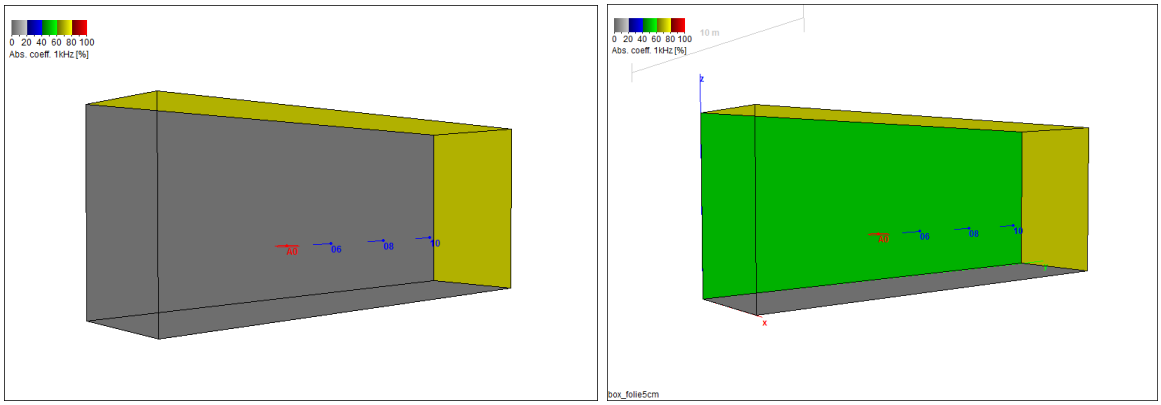

(a) without foil absorbers (b) with foil absorbers, 100 mm distance

Figure 6.5: Rectangular room model with one source and three microphone positions. The color of the walls indicates the absorption coefficient at 1 kHz

is striking that, if using foil absorbers at 100 mm distance to the walls, the sound level decreases approximately twice as fast as in the room with blank walls. Of course, this effect can be expected to be less drastic in larger rooms where the foils are only placed on critical areas.

The flutter echo is clearly observable in the reference curves in form of a pulse train. At the smallest distance of 30 mm, several peaks are still visible, but the curve is much smoother. Increasing the distance between absorber and wall, the peaks decrease and only the peaks of the early reflections stay.

In the impulse responses of the unmodified room, the flutter echo appears in form of a springy, resonance-like sound. Listening to the impulse responses, the difference is audible. The tonal character of the reverberation decreases with growing distance. What stays is the subjective impression of strong early reflections like a flutter echo that decays too fast to have tonal quality.

To see if the foil absorbers would prove their worth in the 16 c building, another simulation was performed. A simplified model was used for the reasons described above (section 6.1). The difference between the simplified model and the previous one is the reduced complexity of the ceiling structure and the top floor, which were modeled as large planes with high scattering values. Also some surfaces, like for instance the doors that are not located directly in the area of measurement, were removed, which made computation much faster. You can see the modified model in figure 6.9.

The source/receiver constellation of the local measurement was used (microphone positions 6 and 8). The results are shown in figure 6.8, where the impulse responses measured at position 6 are shown on the left and the ones measured at position 8 on the right. As a reference, the impulse response without absorbers is shown behind in green color, like in the plots of the rectangular room model. The distances used between foil and wall were 50 mm and 100 mm.

In the reference curve, the pulse train of the flutter is clearly visible. But the difference is less obvious than in the simulation before, although a positive effect can be noticed. The peaks as well as the sound level decrease.

The difference is also not easy to hear. However, maybe due to inadequacies of the model, the flutter echo is not audible very clearly in the reference impulse response, which makes it rather hard to hear the difference. Maybe also the effectiveness of the absorbers was impaired because no absorbers were applied on the door surfaces.

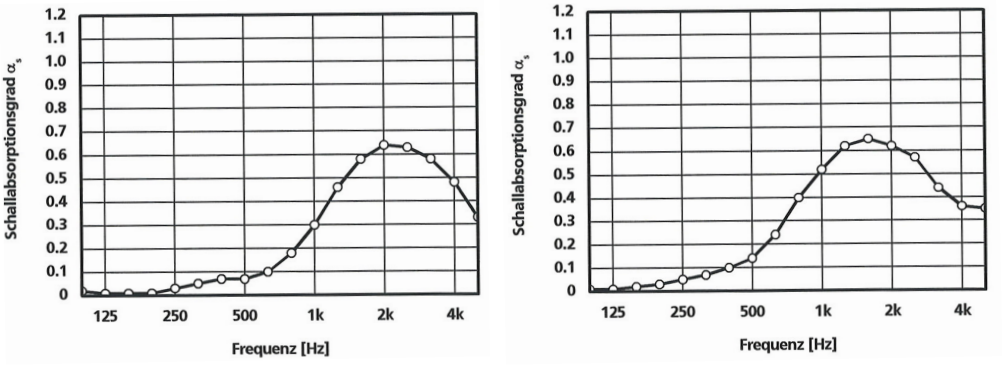

(a) 30 mm distance

(b) 50 mm distance

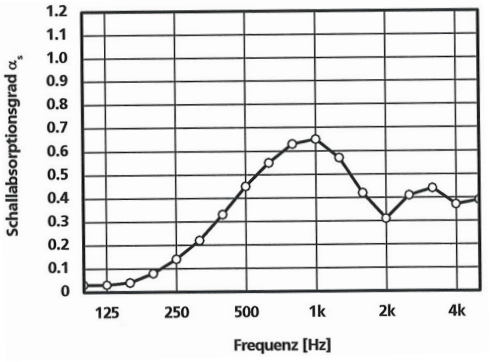

(c) 100 mm distance

Figure 6.6: Absorption coefficients of micro-perforated foil at indicated wall distance. Fraunhofer Institut Bauphysik. [Online], viewed: 25 May 2015, available: http://microsorber.net/service/zertifikate/

6.2.2 Increasing Diffusivity

Additional diffuse reflections can be achieved in various ways. One way is to ensure that parallel walls have a sub-structure that leads to a higher scattering between them by using diffusers or by choice of the surface material.

But instead of reducing the echoes with absorbers or diffusers, it is also possible and might be easier in some special cases to add additional diffuse reflections that mask the echo. Flutter echoes often occur if the wall absorption is distributed irregularly, like in the model in figure 6.5(a). To illustrate this, the absorption coefficients of the front walls and the ceiling in this model where changed. For an absorption of $\alpha = 0.4$ and $\alpha = 0.8$ (full frequency range), the impulse responses are shown in figure 6.10. If the absorption coefficients are doubled, the distinct spikes of flutter echoes emerge. With lower absorption coefficients, the spikes disappear quickly in the diffuse reflections, which decay slower than the flutter echo.

If a uniform distribution of absorption can not be attained, it is better to avoid using unfavorable room geometry. In very large rooms, the air absorption loss can weaken the sound traveling back and forth (above approx. 1 kHz). One might therefore rather have to deal with single echoes, also because of the larger traveling time between the walls.

In building 16 c, one might expect a relatively uniform absorption distribution since all walls are made of concrete. But at narrow passages, the sidewalls are so close compared to all other surfaces (with exception of the floor), that maybe the air absorption between the more distant walls contributes to an irregular absorption distribution, especially if source and receiver are very close together. Long, narrow corridors can often be considered as two-dimensional problems,

since the reflections from the front and rear walls are negligible [21, p. 217]. Therefore, those configurations are very likely to produce flutter echoes.

6.2.3 Avoiding Parallel Walls

The shape of a room has a big influence on its acoustical properties. One effective way of preventing flutter echoes is simply not to use parallel walls. This is also an approach to avoid room modes and therefore often applied to recording spaces. Of course orthogonality is used extensively since the rectangular shape is the indisputable standard concept. However, in architecture, the awareness of the importance of acoustics is constantly growing.

And maybe it does not need radical changes of the shape. In order to find out how subtle changes of the angle between opposite walls affect the flutter echoes, another simulation was performed.

The same model as in section 6.2.1 was used (without absorbers) and also the same source/receiver positions. In steps of 1°, the angle of one of the echo generating walls was increased from 0° to 6° outwards (see illustration 6.11). You can see the results in figure 6.12. The blue curves are the impulse responses in dB for the respective angle indicated by the legend. Each is plotted above the impulse response in green color computed at zero angle. Already an inclination of 1° leads to a visible difference between the impulse responses. The peaks of the flutter are noticeably smaller, and with increasing angle, the impulse responses become even smoother. The difference is audible too. The flutter decreases with increased angle and the reverberation, which quantitatively does not change very much, sounds less colored. This simulation confirms what was already known, namely that the shape of a room has an influence on its acoustics. And this consideration not only affects the design process, but also offers strategies, which can be applied to completed rooms in form of inclined wall coverings. For example, using wooden plates could have the positive side effect of acting as panel absorbers, depending on plate size and thickness. A wall cladding could also be used to guide beneficial early reflections from a speaker to listeners, for example in a conference room situation.

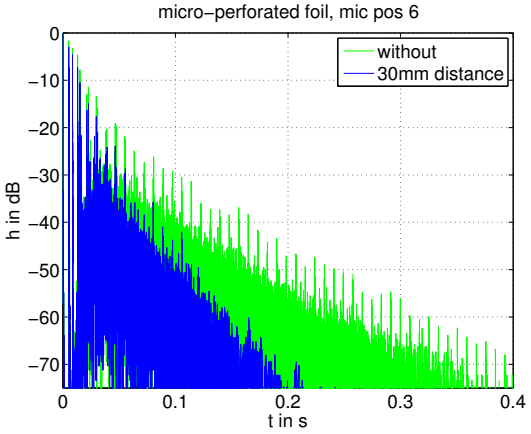

(a) mic. pos. 6, 30 mm distance

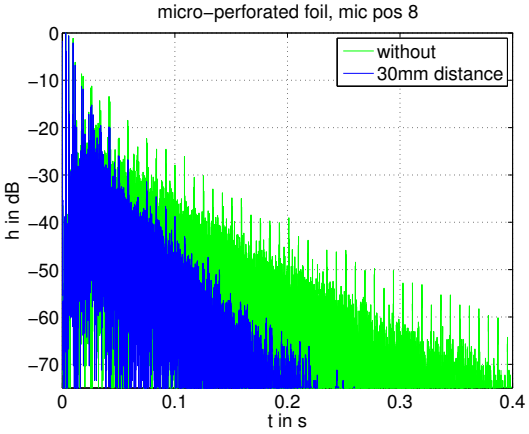

(b) mic. pos. 8, 30 mm distance

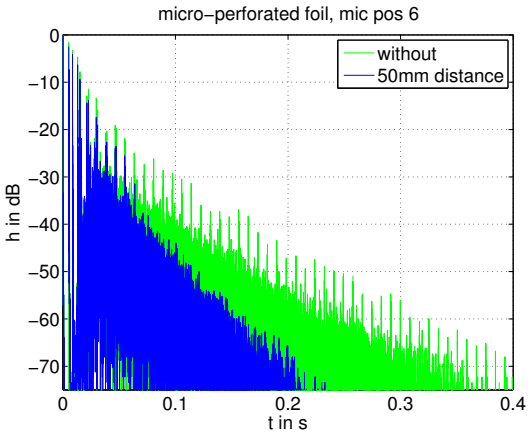

(c) mic. pos. 6, 50 mm distance

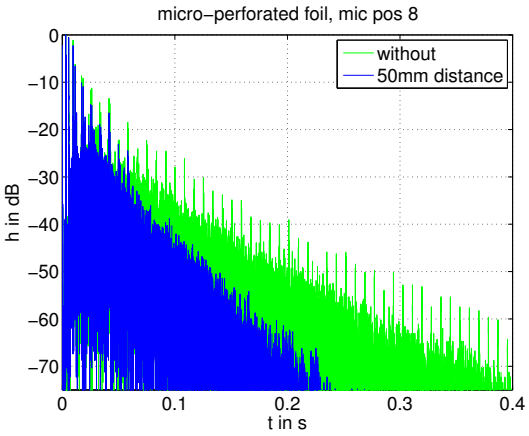

(d) mic. pos. 8, 50 mm distance

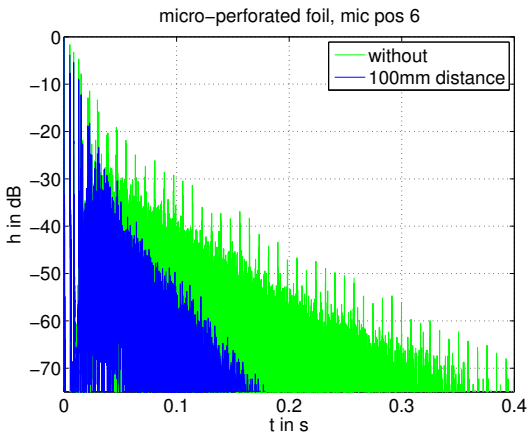

(e) mic. pos. 6, 100 mm distance

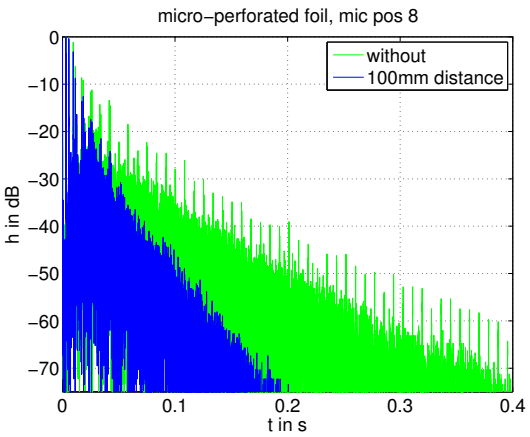

(f) mic. pos. 8, 100 mm distance

Figure 6.7: Impulse response of rectangular room model (green) compared to the ones using foil absorbers (blue)

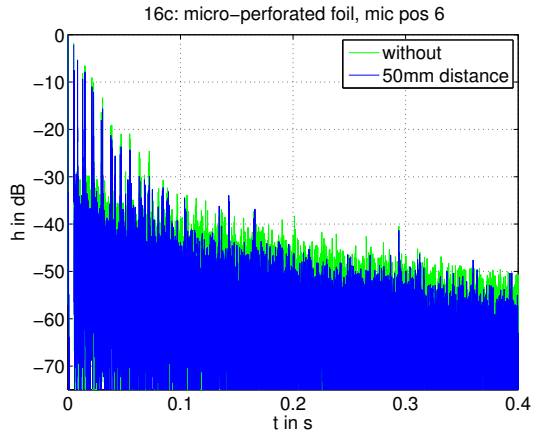

(a) mic. pos. 6, 50 mm distance

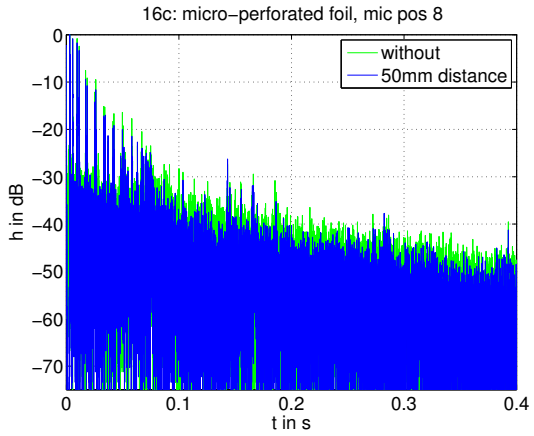

(b) mic. pos. 8, 50 mm distance

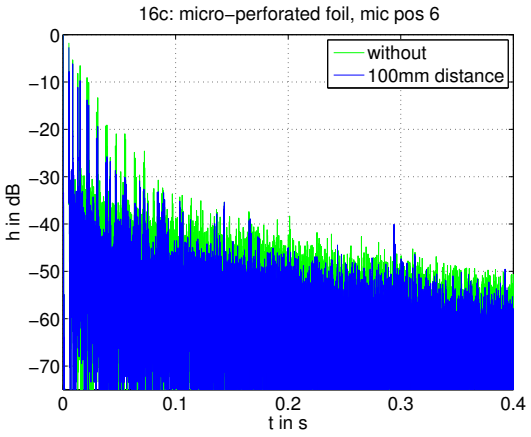

(c) mic. pos. 6, 100 mm distance

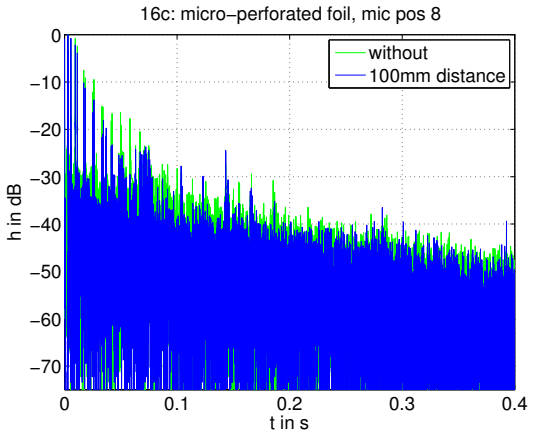

(d) mic. pos. 8, 100 mm distance

Figure 6.8: Impulse response of simplified model of 16 c (green) compared to the ones using foil absorbers (blue)

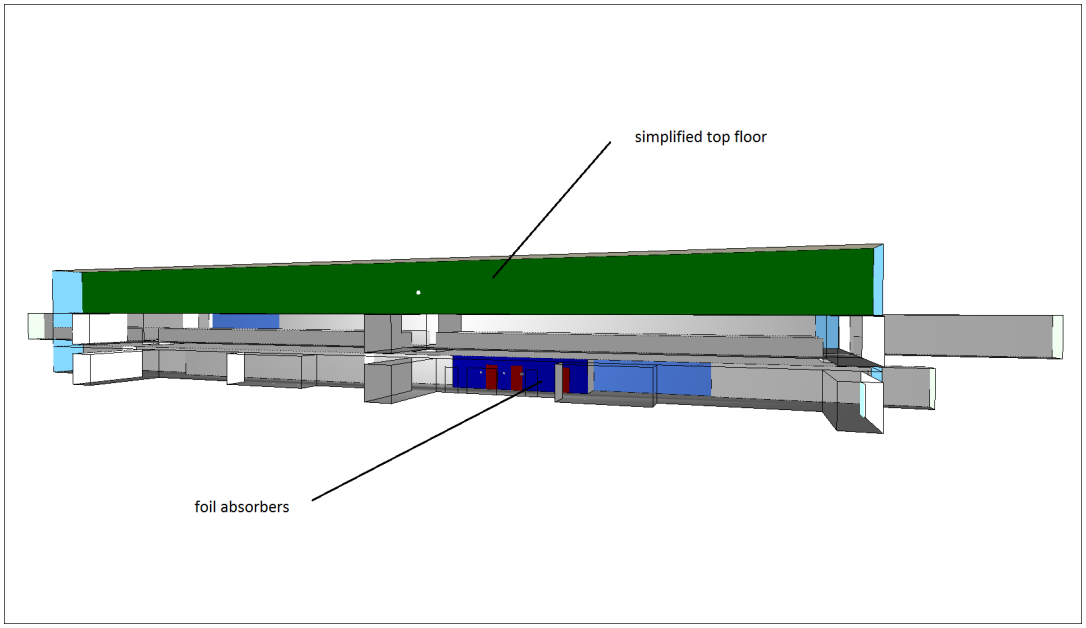

Figure 6.9: Modified model of Inffeldgasse 16 c. The dark blue area indicates the measuring location where the absorbers where applied. The green area is the simplified top floor structure.

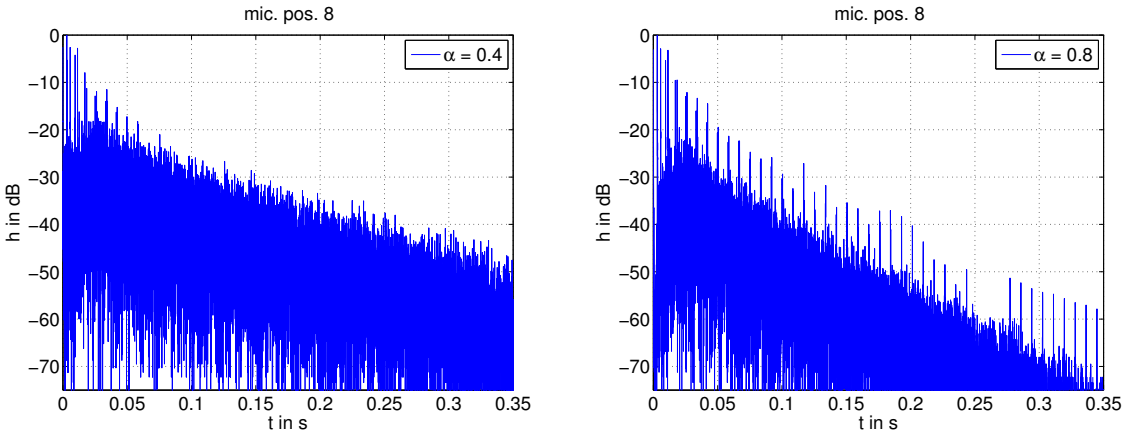

(a) absorption coefficient $\alpha = 0.4$ (b) absorption coefficient $\alpha = 0.8$

Figure 6.10: Masking of flutter echoes by diffuse reflections

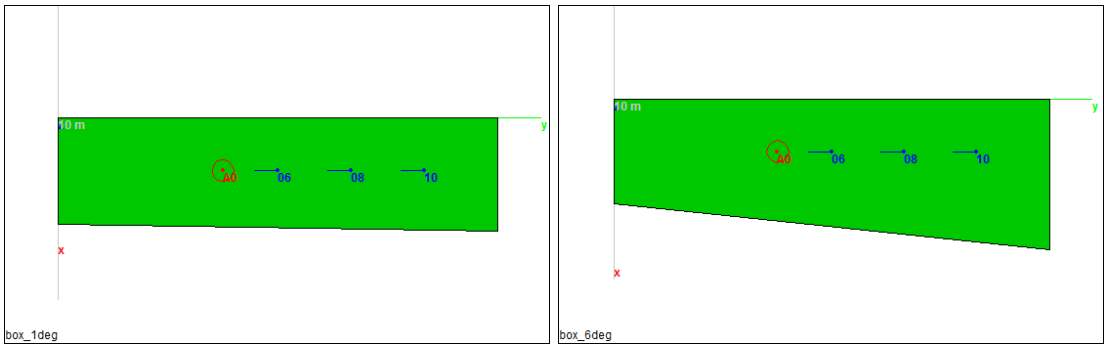

(a) inclination of 1° (b) inclination of 6°

Figure 6.11: Illustration of minimum and maximum inclination angle in rectangular room model

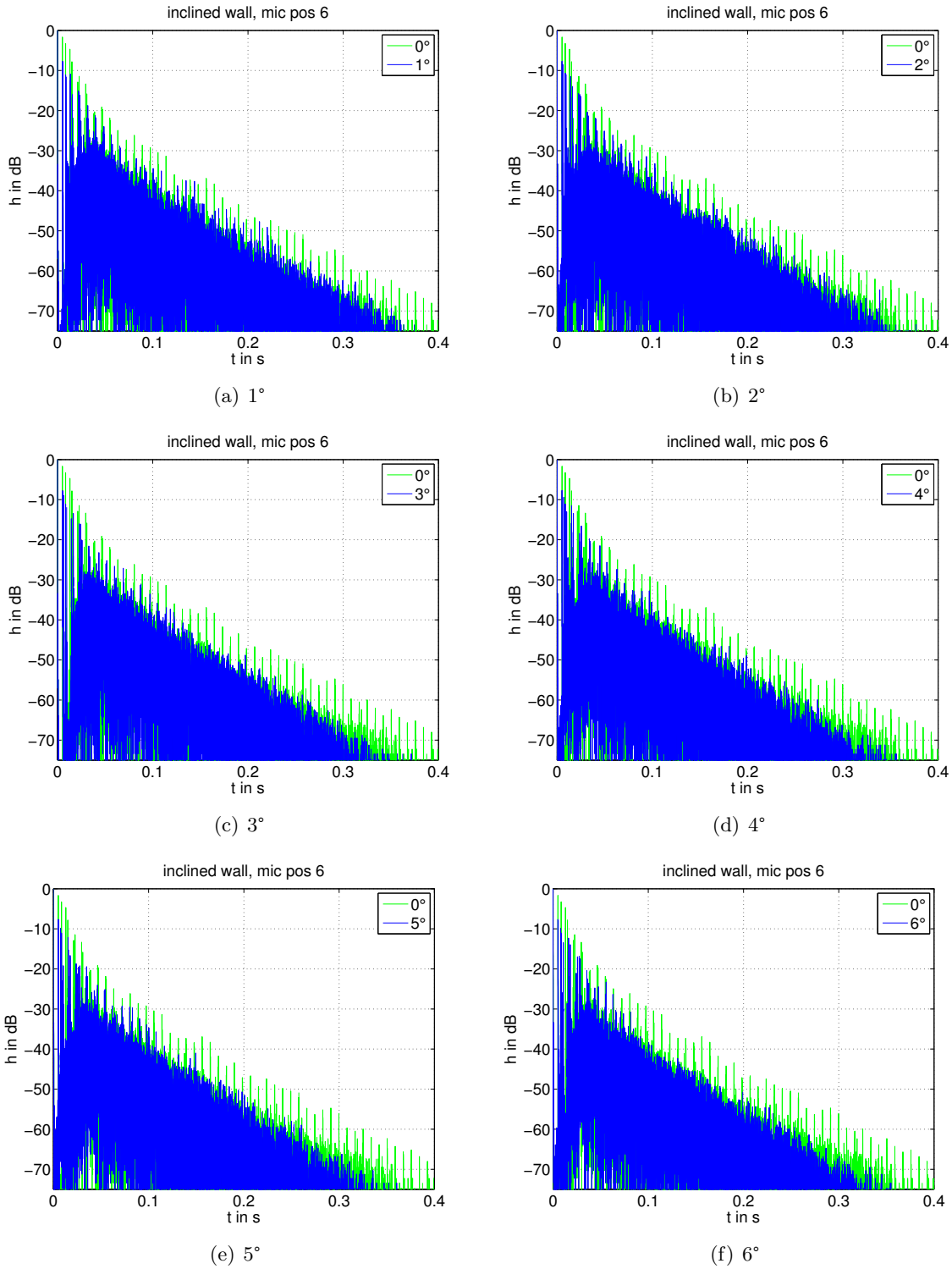

(a) 1° (b) 2°

(c) 3° (d) 4°

(e) 5° (f) 6°

Figure 6.12: Impulse response of rectangular-shaped room compared to the one calculated with one inclined wall for microphone position 6

7 Conclusion

This final chapter serves as a summary of this thesis and contains a discussion of the results.

In chapter 2, the theoretical fundamentals of the topic were explained, starting with the characteristics of sound, and discussing the different approaches of room acoustics. The concept of the reverberation time was described and a general view on the phenomenon of echoes and flutter echoes was provided.

In chapter 3, different measurement methods for acoustic purposes were described. Among other things, classical strategies for measuring the reverberation time, as well as newer strategies that are used to measure the room impulse response were presented, which, due to their various advantages, already have become standard methods.

Finally, the decision has been made to use the MLS method for the following measurements, which were intended to provide an example of measurements in acoustics with special regard to the phenomenon of flutter echoes.

The measurements took place at Inffeldgasse 16 c, where flutter echoes occur at the narrow parts of the corridor. Both a global measurement in the whole ground floor of the building and a local, detailed measurement in an area with clear flutter echoes were performed.

The purpose of the global measurement was to find an acoustical characterization by reverberation time and, if applicable, other measures that are valid for the whole building. This turned out to be difficult, since the measured values are subject to strong local variations. Also, a dependency of the measured reverberation time on the distance between source and receiver has been observed among the results.

The global reverberation time was apparently within the acceptable range defined in *ÖNORM B 8115-3*. But the informative value of this result is debatable. Due to the local variations, the global value might be of limited significance. Furthermore, it could be useful to look at the building as a number of coupled rooms because of the special geometry, which might require a definition of an effective volume and thus the formula for the optimal reverberation time could not be applied, because it is based on the physical volume.

Ultimately, the evaluation has to be made by hearing. Also, the reverberation time is only an auxiliary mean that, of course, cannot include any phenomenon experienced as disturbing. Nevertheless, maybe general measures of reducing the reverberation time would be reasonable in order to improve working conditions, because experience shows that, if a lot of people are inside the building, the sound level rises quickly.

With an acoustic simulation of the building, first, the agreement between the measurement and the building model of Inffeldgasse 16 c was checked. Using the expected absorption and scattering coefficients, a large difference between the measured and the simulated data was found. It turned out to be difficult to fit the simulation with the measurement conditions for evaluation of optimization measures. The finding that, besides the requirement of more sound rays than usual, also many more receiver and source positions would have been required for an assessment of the global situation leads to the suspicion that also the measurement results might not be representative for the whole room. Presumably, this kind of room can hardly be described by a global reverberation time.

Because of these difficulties, further simulations have been made with rectangular room models and a simplified version of the original building model, containing less detailed elements in the areas that are distant from the sources and receivers, which shortened the computation time.

For avoiding flutter echoes, different approaches have been presented. It was shown that the architectural design of the room geometry has a great impact on the occurrence of flutter echoes, as well as other undesirable phenomena like room modes. Sometimes even small changes can already make an important difference. This could be an inclined wall covering that can be used as an absorber, too.

I showed with a simulation, that also very discreet types of absorbers can improve the situation without changing the architectural characteristics of a room very much.

Of course, if classical absorbers are applied, or if different surface materials with very dissimilar absorption values are used, an even distribution of the absorption is beneficial. Echoes are mostly audible, only because too few diffuse reflections are produced, which otherwise could mask the echo.

Bibliography

[1] S. Weinzierl, *Handbuch der Audiotechnik*. Berlin: Springer, 2008.

[2] G. Graber, W. Weselak, "Raumakustik, Version 5.3," Institute of Broadband Communications, Graz University of Technology, 2009, lecture notes.

[3] M. Dickreiter, *Handbuch der Tonstudiotechnik*, 7th ed., ARD.ZDF medienakademie, Ed. München: K. G. Saur, 2008, vol. 1.

[4] S. Plagg, M. Pobitzer, "Eigenfrequenzen - Eigenmoden Resonanzfrequenzen - Raummoden," Bachelor Thesis, Graz University of Technology, 2011.

[5] R. Lerch, *Technische Akustik*. Berlin: Springer, 2009.

[6] M. Möser, *Technische Akustik*, 9th ed. Berlin: Springer Vieweg, 2012.

[7] L. Cremer, *Die Wissenschaftlichen Grundlagen der Raumakustik*, 2nd ed. Stuttgart: S. Hirzel Verlag, 1978, vol. 1.

[8] L. Cremer, *Die Wissenschaftlichen Grundlagen der Raumakustik*. Stuttgart: S. Hirzel Verlag, 1948, vol. 1.

[9] D. Maa, "The Flutter Echoes," *J. Acoust. Soc. Amer.*, vol. 13, pp. 170–178, 1941.

[10] "Raumakustik, Anhang A," Institute of Broadband Communications, Graz University of Technology, lecture notes for room acoustics laboratory.

[11] *Acoustics - Application of new measurement methods in building and room acoustics*, ÖNORM EN ISO 18233, 2006.

[12] M. Vorlaender, H. Bietz, "Comparison of Methods for Measuring Reverberation Time," *Acta Acustica united with Acustica*, vol. 80, no. 3, pp. 205–215, 1994.

[13] *Acoustics - Measurement of room acoustic parameters - Part 2: Reverberation time in ordinary rooms*, ÖNORM EN ISO 3382-2, 2009.

[14] W. Weselak, "Akustische Messtechnik, Version 8.0," Institute of Signal Processing and Speech Communication, Graz Universitiy of Technology, 2013, lecture notes.

[15] S. Müller, P. Massarani, "Transfer-function measurement with sweeps," *J. Audio Eng. Soc*, vol. 49, no. 6, pp. 443–471, 2001. [Online]. Available: http://www.aes.org/e-lib/browse.cfm?elib=10189

[16] G. Stan, J. Embrechts, "Comparison of different impulse response measurement techniques," *J. Audio Eng. Soc.*, vol. 50, pp. 249–262, 2002.

[17] A. Wendemuth, *Grundlagen der digitalen Signalverarbeitung*. Berlin: Springer, 2005.

[18] M. Schröder, "New Method of Measuring Reverberation Time," *J. Acoust. Soc. Amer.*, vol. 37, pp. 409–412, 1965.

[19] *Acoustics- Measurement of room acoustic parameters - Part 1: Performance spaces*, ÖNORM EN ISO 3382-1, 2009.

[20] P. Gutmann, "Nachhallakustik langgestreckter Räume," Project, Graz University of Technology, 2007.

[21] L. Cremer, *Die Wissenschaftlichen Grundlagen der Raumakustik.* Stuttgart: S. Hirzel Verlag, 1950, vol. 3.

[22] *Sound insulation and architectural acoustics in building construction - Part 3: Architectural acoustics*, ÖNORM B 8115-3, 2005.

[23] H. Kuttruff, "Über Autokorrelationsmessungen in der Raumakustik," *Acta Acustica united with Acustica*, vol. 16, no. 3, pp. 166–174, 1965.

[24] K. Środecki, "Evaluation of the Reverberation Decay Quality in Rooms Using the Autocorrelation Function and the Cepstrum Analysis," *Acustica*, vol. 80, pp. 216–225, 1994.

[25] L. Dietsch, "Objektive raumakustische Kriterien zur Erfassung von Echostörungen und Lautstärke bei Musik und Sprachdarbietungen," Ph.D. dissertation, Technical University of Dresden, 1983.

[26] A. Roy, F. Gimbott, "Automatic Echo Determination in Measured Impulse Responses," *preprint of the Audio Eng. Soc. 94th Conv.*, Berlin, 1993.

[27] J. Abel, P. Huang, "A Simple, Robust Measure of Reverberation Echo Density," *proc. of the Audio Eng. Soc. 121st Conv.*, San Francisco, 2006.

[28] P. Rubak, R. Johansen, "Coloration in Natural and Artificial Room Impulse Responses," *proc. of the Audio Eng. Soc. 23rd Int. Conf.*, Copenhagen, 2003.